Journal of Medicinal Chemistry

Article

pubs.acs.org/jmc

A SAR Study of Novel Antiproliferative Ruthenium and Osmium Complexes with Quinoxalinone Ligands in Human Cancer Cell Lines

Werner Ginzinger,[†] Gerhard Mühlgassner,[†] Vladimir B. Arion,*[,†] Michael A. Jakupec,[†] Alexander Roller,[†] Markus Galanski,[†] Michael Reithofer,[†] Walter Berger,[‡] and Bernhard K. Keppler*[,†]

[†]University of Vienna, Institute of Inorganic Chemistry, Währinger Strasse 42, A-1090 Vienna, Austria

[‡]Medical University of Vienna, Department of Medicine I, Institute of Cancer Research, Borschkeg. 8a, A-1090 Vienna, Austria

Supporting Information

ABSTRACT: A series of ruthenium(II) arene complexes with 3-(1*H*-benzimidazol-2-yl)-1*H*-quinoxalin-2-one, bearing pharmacophoric groups of known protein kinase inhibitors, and related benzoxazole and benzothiazole derivatives have been synthesized. In addition, the corresponding osmium complexes of the unsubstituted ligands have also been prepared. The compounds have been characterized by NMR, UV−vis, and IR spectroscopy, ESI mass spectrometry, elemental analysis, and by X-ray crystallography. Antiproliferative activity in three human cancer cell lines (A549, CH1, SW480) was determined by MTT assays, yielding IC_{50} values of 6−60 μM for three unsubstituted metal-free ligands, whereas values for the metal complexes vary in a broad range from 0.3 to 140 μM. Complexation with osmium of quinoxalinone derivatives with benzimidazole or benzothiazole results in a more consistent increase in cytotoxicity than complexation with ruthenium. For selected compounds, the capacity to induce apoptosis was confirmed by fluorescence microscopy and flow-cytometric analysis, whereas cell cycle effects are only moderate.

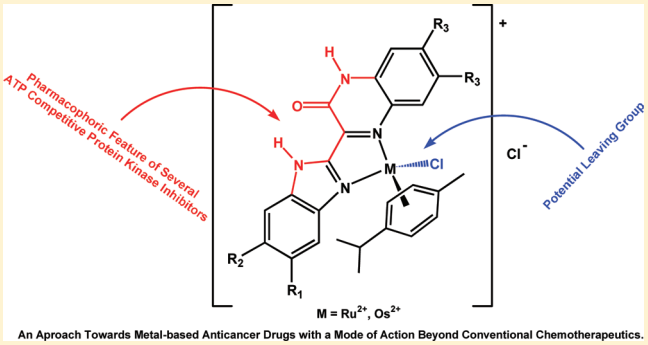

An Aproach Towards Metal-based Anticancer Drugs with a Mode of Action Beyond Conventional Chemotherapeutics.

INTRODUCTION

Since the approval of cisplatin for the treatment of cancer, a number of other metal complexes have been investigated for their therapeutic potential.[1−3] Among them, ruthenium compounds have received respectable attention because of interesting features such as iron mimicking behavior or the availability of several oxidation states under physiological conditions.[4] Two ruthenium compounds, [ImH] *trans*-[$RuCl_4$(Im)(dmso-*S*)] (NAMI-A, Im = imidazole) and [IndH] *trans*-[$RuCl_4$(Ind)$_2$)] (KP1019, Ind = 1*H*-indazole), have successfully completed phase I clinical trials.[5−7] NAMI-A has already entered a phase II study.[8] Recently, half-sandwich ruthenium(II) and osmium(II) arene compounds were discovered as a new class of potential anticancer drugs.[9,10] The arene ligand stabilizes the oxidation state +II at the metal center. Furthermore, the metal−arene moiety is believed to facilitate uptake by diffusion through the cell membrane. In some cases, the arene ligand may also play a crucial role in the interaction with intracellular targets (e.g., intercalation with DNA).[11] The remaining three coordination sites are occupied by monodentate or chelating ligands, which control the reactivity toward biomolecules and thereby the mode of action of the drug.[12−16]

Protein kinases are involved in the regulation of most cellular processes, such as metabolism, proliferation, damage repair, and apoptosis. Perturbations of these signaling pathways are quite common in cancer cells.[17] Therefore efforts have been made to intervene therapeutically with kinase inhibitors to block either the kinase−substrate interaction or the ATP binding site.[18,19] Recently, Meggers and co-workers developed a new class of metal-based kinase inhibitors inspired by the ATP competitive staurosporine molecule (Figure 1).[20−23] The metal within these rather inert complexes serves as a scaffold for shaping the molecule. Some new inhibitors show high selectivity and overcome resistance by irreversible covalent binding to the target.[24] In this context, coordination might provide a new mode of action so that keeping at least one moderately reactive site could be advantageous in some cases.

In China, chronic myelocytic leukemia has commonly been treated with the traditional recipe Danggui Longhui Wan, a mixture of 11 herbal medicines. The ingredient *Indigo naturalis* was suggested to be responsible for the antileukemic effects. Finally, the activity was attributed to a minor constituent of the blue powder, namely the red-colored isomer of indigo, indirubin (Figure 2a), which was found to inhibit cyclin dependent kinases.[25,26] In the meantime not only a large number of derivatives has been synthesized, but also other targets have been identified.[27−32] The crystal structure of Thr-160 phospho-CDK2-cyclin A with indirubin-5-sulfonate revealed that the inhibitor binds to the ATP binding site of the protein through the lactam moiety and the N$^{1'}$−H group by

Received: January 20, 2012
Published: March 15, 2012

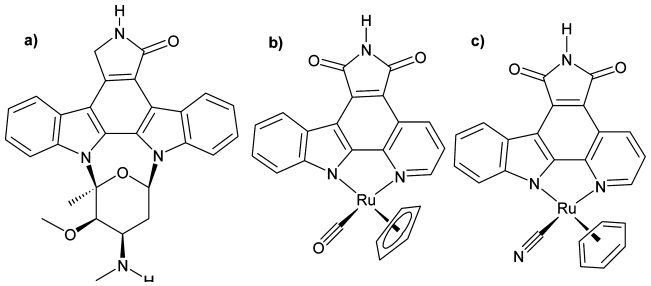

Figure 1. Staurosporine (a) and new metal-based kinase inhibitors developed by Meggers et al.[20−23] (b,c).

formation of three hydrogen bonds.[33] A similar pharmacophoric group, which is a basic structural element of promising tyrosine kinase inhibitors, is present in 4-amino-3-(1*H*-benzimidazol-2-yl)-1*H*-quinolin-2-ones (Figure 2b)[34−36] and in 3-(3-amino-1*H*g f-indol-2-yl)-1*H*-quinoxalin-2-ones (Figure 2c).[37,38]

Combining the structures of the benzimidazolylquinolinone and the indolylquinoxalinone in Figure 2 to the motif of 3-(1*H*-benzimidazol-2-yl)-1*H*-quinoxalin-2-one results in a compound that incorporates the indirubin pharmacophore together with a vicinal diimine, which should be well suited for coordination to metal ions. Using Kröhnke intermediates, this compound type has already been synthesized by Westphal et al.[39,40] Besides the benzimidazole derivative, they prepared the corresponding benzoxazole and benzothiazole analogues in the same way. Herein we present new synthetic approaches for the family of 3-(benzazol-2-yl)-1*H*-quinoxalin-2-ones and the first evaluation of their antiproliferative potency. The benzimidazole derivative was compared with the corresponding azoles containing oxygen and sulfur. In addition, chloro and methyl substituents with inverse inductive effects on the electron density of the aromatic system were introduced at the benzene moieties in order to explore some structure−activity relationships. However, the solubility of the heterocyclic substances is extremely poor. Coordination to an organometallic ruthenium(II) and osmium (II) arene scaffold should not only diminish this problem but may also help to enhance anticancer activity. To elucidate the influence of the metal, the structures of corresponding ruthenium and osmium complexes were examined by X-ray diffraction and compared with the metal-free ligands. Moreover, the impact of the metal on the reactivity of the monodentate chlorido ligand was studied by monitoring aquation and backward anation. Structure−activity relationships were elucidated by means of the MTT assay in three human cancer cell lines, and effects of selected compounds on the cell cycle were investigated by flow cytometry. Furthermore, induction of apoptosis was proved by fluorescence microscopy.

RESULTS AND DISCUSSION

Syntheses of Ligands and Complexes. Because the reported pathways to the ligands studied in this work turned out to be not very reliable in terms of reproducibility and yields, new synthetic strategies were developed. 3-(1*H*-Benzimidazol-2-yl)-1*H*-quinoxalin-2-one, its derivatives, and oxazole analogues were synthesized in four steps. By reaction of ethyl 2-(ethoxycarbonyl)acetimidate hydrochloride (**1**) with suitable 1,2-phenylenediamines or 2-aminophenols cyclization products, **2a−f** have been obtained. Bromination of the α-methylene group in acetic acid resulted in **3a−f**. This reaction requires a high quality of acetic acid and sodium acetate. The dibromo derivatives are quite unstable and could not be purified. The dimethyl compound **2c**, being a stronger base than the other intermediates, partly formed a salt with acetic acid, which may account for higher contaminations of **3c**. The following cyclization with suitable 1,2-phenylenediamines led to the ligands **4a−k** (Scheme 1a). Alternatively, **4a** was synthesized by condensation of ethyl 3-oxo-3,4-dihydro-quinoxaline-2-carboxylate and 1,2-phenylenediamine in ethylene glycol under argon at 170 °C. However, this pathway could only be applied successfully to the unsubstituted compound, although with a much lower yield. The corresponding thiazole analogues were synthesized by another approach because bromination of ethyl 2-(benzothiazol-2-yl)acetate led to prevalent formation of side products. First, diethyl sodium oxalacetate was condensed with 1,2-phenylenediamines to give **5a−b**. Then ester hydrolysis and nitrosation followed by decarboxylation[41] afforded **6a** and **6b** (Scheme 1b). Finally, the oximes were converted into the corresponding benzothiazoles **4l−o** using 2-mercaptoanilines. The ^{1}H NMR spectrum of the crude product **4l** displayed a 1:1:1 triplet of ammonium, which indicated that the expected intermediate 2,3-dihydrobenzothiazole is oxidized to benzothiazole by the initially released hydroxylamine. Only in the case of **4o** oxygen atmosphere for completion of the oxidation reaction was necessary.

The low solubility of the ligands in suitable organic solvents precluded the use of chromatographic methods or straightforward recrystallization procedures for their further purification. **4a** was dissolved in acetic acid and reprecipitated by addition of diethylether, followed by dissolution in orthophosphoric acid and reprecipitation with NaOH. To remove inorganic salts, the suspended compound was boiled in water. It should be noted that hydrochlorides of all benzimidazole derivatives are rather poorly soluble too. **4h** was recrystallized from ethylene glycol. However, to remove traces of this solvent, treatment in boiling methanol was necessary. **4l** was dissolved in a mixture of ethanol and THF and precipitated by pouring the solution into a huge amount of water. Afterward, the compound was recrystallized from *o*-xylene. Finally, **4l** was dissolved in THF and precipitated with water. Because the compound possesses poor solubilities, all steps required large volumes of solvents.

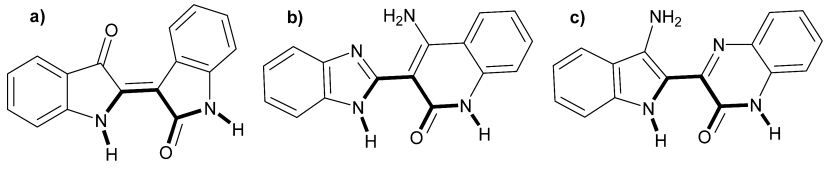

Figure 2. ATP competitive protein kinase inhibitors with the same pharmacophore: (a) indirubin, (b) 4-amino-3-(1*H*-benzimidazol-2-yl)-1*H*-quinolin-2-one, (c) 3-(3-amino-1*H*-indol-2-yl)-1*H*-quinoxalin-2-one.

dx.doi.org/10.1021/jm3000906 | *J. Med. Chem.* 2012, 55, 3398−3413

Scheme 1. Novel Synthetic Pathways to Ligands 4a–k (a) and 4l–o (b)[a]

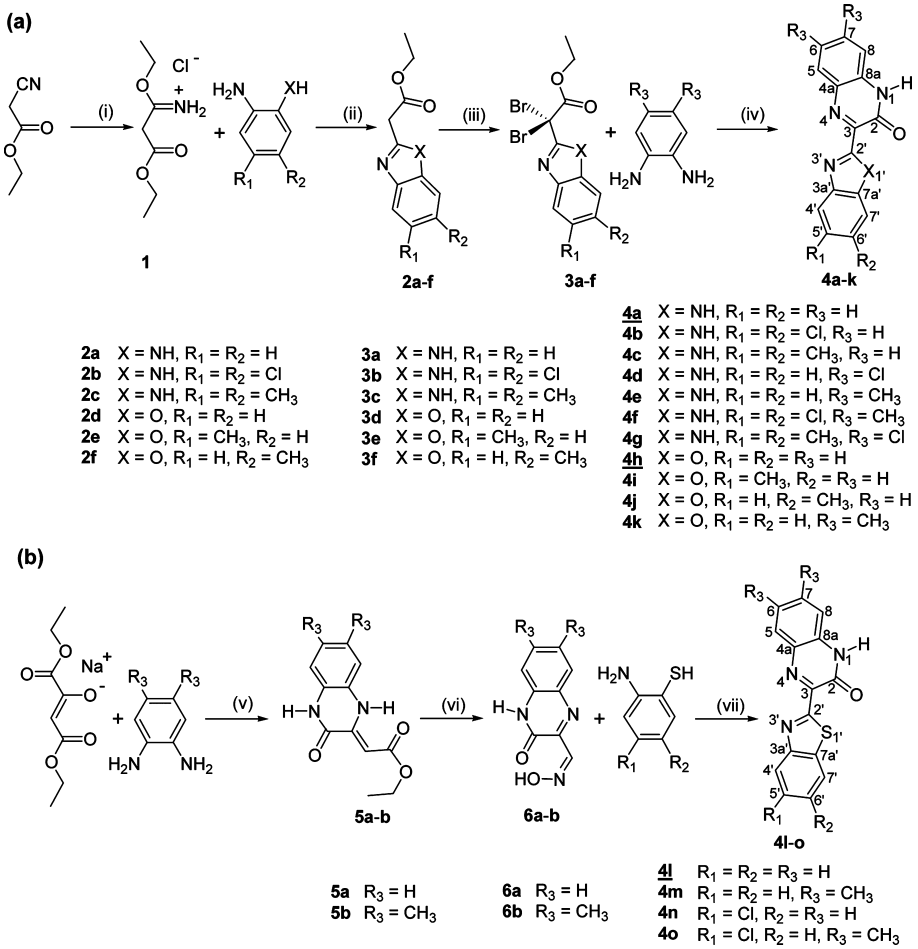

[a]Reagents and conditions: (i) $EtOH/H_2O$, $SOCl_2$, Ar, 0 °C–rt. (ii) $MeOH_{abs}$, Ar, Δ. (iii) AcOH, NaOAc, Br_2, Ar, rt. (iv) $EtOH_{abs}$, NaOAc, Ar, Δ. (v) AcOH. (vi) NaOH, Δ, $NaNO_2$, H_2SO_4. (vii) EtOH, HCl. Compounds with underlined numbers were characterized by X-ray diffraction.

Therefore all ligands with exception of the three biologically tested derivatives were used for complexation without extensive purification.

The quinoxalinone ligands were reacted with 0.5 equiv of the dimeric bis[chlorido(μ-chlorido)(η^6-*p*-cymene)ruthenium(II)] (**7a**) or bis[chlorido(μ-chlorido)(η^6-*p*-cymene)osmium(II)] (**7b**) in absolute ethanol at 70 °C. Normally, the presence of small amounts of concentrated hydrochloric acid improved the quality and the yield of the products. Some complexes were isolated by filtration from the cooled reaction mixture, while the others were precipitated by addition of diethyl ether or other solvents. For purification, the organometallic compounds were dissolved in highly diluted hydrochloric acid, or in some cases just in water, filtered, and the filtrates immediately frozen and lyophilized afterward. The ruthenium η^6-benzene complex **10a** (an analogue of **8a**) was prepared similarly to the *p*-cymene derivatives.

Characterization of Compounds. Positive ion ESI mass spectra of the ligands **4a**, **4h**, and **4l** displayed strong peaks of the ions $[M + Na]^+$ and $[2M + Na]^+$. While the spectrum of **4a** contains a peak with *m*/*z* 263 attributed to $[M + H]^+$, the formation of such ions was not observed for **4h** and **4l**. However, the mass spectra of the latter measured in the negative ion mode showed peaks which have been assigned to the ions $[M - H]^-$ and $[2M - 2H + Na]^-$. The peak attributed to $[RuCl(arene)L]^+$ was found for all ruthenium complexes with the exception of **8b** and **8d**. $[RuCl(arene)L - HCl]^+$ and $[RuCl(arene)L - H + Na]^+$ ions are also abundant (Scheme 2). For osmium-containing complexes, similar mass spectra have been obtained. Peaks with higher *m*/*z* values were also

Scheme 2. Synthesis of Complexes 8a–o, 9a, 9h, and 9l[a]

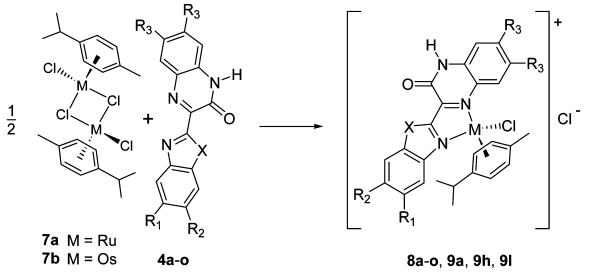

8a M = Ru, X = NH, R1 = R2 = R3 = H
8b M = Ru, X = NH, R1 = R2 = Cl, R3 = H
8c M = Ru, X = NH, R1 = R2 = CH3, R3 = H
8d M = Ru, X = NH, R1 = R2 = H, R3 = Cl
8e M = Ru, X = NH, R1 = R2 = H, R3 = CH3
8f M = Ru, X = NH, R1 = R2 = Cl, R3 = CH3
8g M = Ru, X = NH, R1 = R2 = CH3, R3 = Cl
8h M = Ru, X = O, R1 = R2 = R3 = H
8i M = Ru, X = O, R1 = CH3, R2 = R3 = H
8j M = Ru, X = O, R1 = H, R2 = CH3, R3 = H
8k M = Ru, X = O, R1 = R2 = H, R3 = CH3
8l M = Ru, X = S, R1 = R2 = R3 = H
8m M = Ru, X = S, R1 = R2 = H, R3 = CH3
8n M = Ru, X = S, R1 = Cl, R2 = R3 = H
8o M = Ru, X = S, R1 = Cl, R2 = H, R3 = CH3
9a M = Os, X = NH, R1 = R2 = R3 = H
9h M = Os, X = O, R1 = R2 = R3 = H
9l M = Os, X = S, R1 = R2 = R3 = H

[a]Reagents and conditions: $EtOH_{abs}$, Ar, 70 °C. Compounds with underlined numbers were characterized by X-ray diffraction.

dx.doi.org/10.1021/jm3000906 | J. Med. Chem. 2012, 55, 3398–3413

registered but could not be unequivocally identified. UV−vis spectra of metal-free and metal-based compounds in methanol (Figures S1−S4, Supporting Information) display several structured bands, which were characterized by their first derivatives. NMR spectra were recorded in DMSO-d_6 with exception of complexes with oxazole derivatives and **10a** (with η^6-bound benzene), which decompose in this medium very fast. Therefore, in those cases, MeOH-d_4 was used as a solvent. Sometimes even for complexes with benzimidazole and benzothiazole derivatives a very slow dissociation in DMSO-d_6 with liberation of the metal-free quinoxalinone ligand and formation of [$RuCl_2$(*p*-cymene)(dmso)] was observed. Frequently, directly after dissolution the signals in ^{1}H NMR spectra appeared as quite broad lines and their resolution into multiplets was found to be time-dependent. Consequently, the ^{1}H NMR spectra were usually recorded once more after all other experiments. ^{1}H,^{1}H-ROESY spectra facilitated the assignment of resonances in the case of metal-based compounds by showing NOE interactions between *p*-cymene and quinoxalinone ligands. These were particularly helpful for discerning C^5 and C^8 or $C^{4\prime}$ and $C^{7\prime}$ because cross-peaks for long-range coupling between N^1H and C^8 or C^{4a} were not always detectable. In the case of **8a**, a ^{1}H,^{13}C-HSQC-TOCSY was performed for unambiguous distinction of carbons to which four protons with δ at 7.50−7.21 ppm (Figure S5, Supporting Information) were attached. The ^{1}H,^{13}C-HMBC of **8e** showed cross-peaks from $N^{1\prime}$H to C^3 and $C^{3a\prime}$, while in the ^{1}H,^{15}N-HMBC, besides the cross-peak belonging to C^5H and N^4 with a ^{15}N shift of 248.8 ppm, another, actually very weak peak at 135.1 ppm was found, pointing to C^8H. This was confusing because ^{1}H,^{15}N-HSQC spectrum, measured with 128 scans, showed only one signal at about 135 ppm for $N^{1\prime}$. A repeated measurement with 768 scans, however, delivered two cross-peaks with ^{15}N shift of 134.6 ppm ($N^{1\prime}$) and 135.1 ppm (N^1) (Figures S6−S9, Supporting Information). Often, compounds did not give any peak in ^{1}H,^{15}N-HSQC due to very broad NH-signals. In many cases, comparison of the spectra for differently substituted derivatives was required to ensure a correct assignment. Generally, a downfield shift of ^{1}H resonances of the coordinated ligands, compared to those of the uncoordinated ones, has been observed. Thereby ruthenium shows a more pronounced effect than osmium. For recently described maltol derived ruthenium *p*-cymene complexes, the diastereotopic signal pattern of the four aromatic *p*-cymene protons is lost on going from aprotic to protic solvents, indicating a fast inversion at the metal center there.[42] However, this was not the case for the compounds presented here.

Interconversion of Chlorido- and Aqua-Species. The behavior of **8a** in aqueous solution was monitored by ^{1}H NMR spectroscopy. Figure 3 shows the time dependence of the NMR spectra. The result suggests a hydrolysis of the Ru−Cl bond and the formation of the monoaqua species in aqueous solution.

Attempts to prepare the monoaqua species by treatment of the initial chlorido complex with $AgNO_3$ in D_2O failed because of abundant formation of side products. Therefore, [Ru(*p*-cymene)(**4a**)(H_2O)](NO_3)$_2$ (**11a**) was prepared by an alternative route. First, the chlorido-bridged dimer **7a** was treated with silver nitrate in water. After removal of silver chloride, the intermediate was allowed to react in situ with **4a** to form **11a**. The corresponding aqua complexes (**11h**, **11l**, **12a**, **12h**, and **12l**) of **8h**, **8l**, **9a**, **9h**, and **9l** were prepared

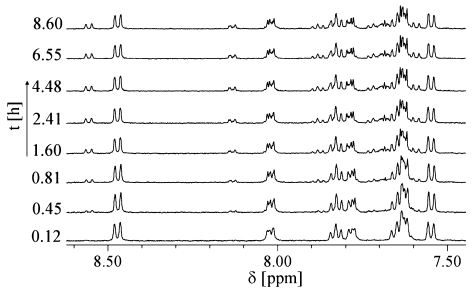

Figure 3. Time-dependent changes of NMR spectra of **8a** in D_2O.

similarly. The batches were still slightly contaminated but used for investigations of the reactions with chloride and the pH dependent behavior without further purification. Their ^{1}H resonances agree well with those for the species generated upon aquation of the corresponding chlorido complexes.

The reaction of **11a** with sodium chloride in D_2O monitored by integration of the doublets at 8.56 and 8.47 ppm demonstrated the reversibility of the aquation. The hydrolysis of the compounds occurred markedly slower than that of recently reported maltol-derived organometallic complexes, where a complete aquation within seconds was observed.[43] This is in agreement with earlier observations, that ruthenium arene complexes containing N-donor ligands normally display a slower hydrolysis, than those with O- and/or S-donor atoms.[44,45]The aquation of the osmium analogue **9a** and the reverse anation reaction of the aqua complex **12a** with sodium chloride are even slower, in accord with results published elsewhere.[46]

The quality of the data did not allow a reliable calculation of the rate constants because fitting with a model including pseudo-first-order kinetics for aquation and second-order kinetics for backward anation did not give adequate results. Especially, for the chloride concentration in the backward reaction, a fractional order is quite conceivable. Nonetheless, the rate of the conversion of the chlorido-species into the aqua-species complies with the following order: benzoxazole derivative > benzimidazole derivative > benzothiazole derivative. The rate is markedly higher for ruthenium complexes than that for the corresponding osmium analogues (Figures 4−5, S10−S14 of Supporting Information). It should be also stressed that in isotonic saline the amount of the aqua complex in equilibrium is negligible.

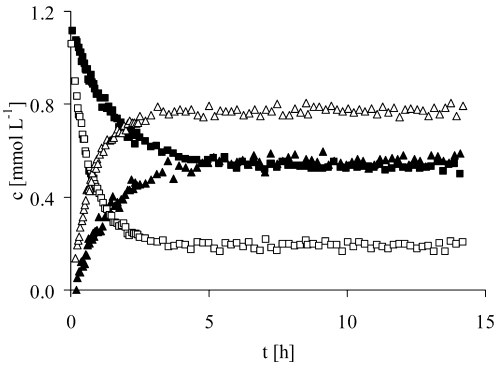

Figure 4. NMR monitored reaction of **11a** with NaCl in D_2O at 298 K. (□) Aqua species in 4.2 mM NaCl. (Δ) Formed chlorido species in 4.2 mM NaCl. (■) Aqua species in 1.4 mM NaCl. (▲) Formed chlorido species in 1.4 mM NaCl.

dx.doi.org/10.1021/jm3000906 | J. Med. Chem. 2012, 55, 3398−3413

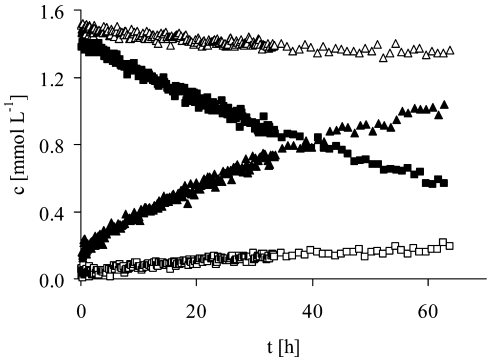

Figure 5. NMR monitored aquation of **9a** in D_2O at 298 K. (□) Formed aqua species. (Δ) Chlorido species. Reaction of **12a** with NaCl in D_2O: (■) aqua species in 4.3 mM NaCl. (▲) Formed chlorido species in 4.3 mM NaCl.

pK_a Values. Attempts to estimate pK_a values by titrations of the aqua complexes with a base monitored by NMR spectroscopy revealed a complex dependence of the chemical shift on pD as shown for **11a** (aquation product of **8a**, Figure 6).

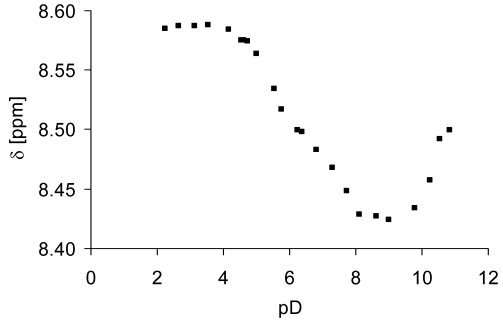

Figure 6. pD dependence of a ^{1}H NMR chemical shift (most probably C^{5}H) of **11a** in D_2O, titrated with DNO_3 and NaOD.

The shape of the curve suggests three pK_a values, the first at pD 5–6, the second at pD 7–8, and the third at pD 10–11. To verify these findings, titrations monitored by UV–vis spectroscopy were performed. The form of the UV–vis titration curves is strongly affected by other species present in solution (e.g., perchlorate, triflate, or chloride, sodium or potassium, Figure 7). In the case of chloride-free medium, the results are generally

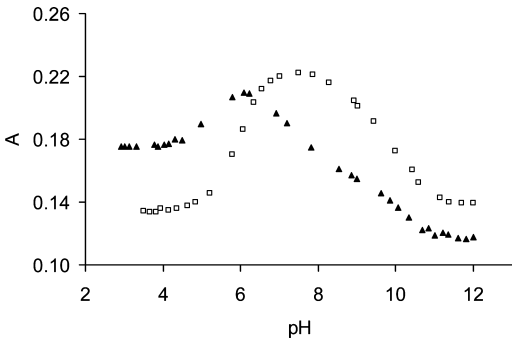

Figure 7. pH dependence of the absorbance at 490 nm. (▲) 2.3 × 10^{-5} mM **11a** in H_2O acidified with $HClO_4$ to pH 3, titrated with KOH. (□) 2.2 × 10^{-5} mM **8a** in aqueous 1 M KCl acidified with HCl to pH 3, titrated with KOH.

in accord with the NMR data. Even for the chlorido species **8a**, a deprotonation step at pH 4–8 is plausible, which is responsible for the dramatic decrease of the solubility from 20 mg mL^{-1} in H_2O to 0.15 mg mL^{-1} in phosphate buffered saline (pH 7.2) due to formation of a nonelectrolyte complex. Comparison with the corresponding oxazole- and thiazole-derivatives (solubilities: **8h**, 7.7 mg mL^{-1} in H_2O, 1.1 mg mL^{-1} in PBS; **8l**, 7.0 mg mL^{-1} in H_2O, 0.48 mg mL^{-1} in PBS; see titration curves in the Figures S15–S20, Supporting Information) indicates that between pH 4 and 8 both the aqua ligand and the amide of the quinoxalinone are deprotonated, although for the unsubstituted 2-quinoxalinone, a pK_a of 9.2 was reported.[47] The third deprotonation step observed for the benzimidazole derivatives was tentatively assigned to the N^1′H group.

Only the NMR titration curves of the osmium complex **12l** (aquation product of **9l**) showed a sigmoidal form expected for one deprotonation step. The solubility of **9l** decreased only by a factor of 5.5 from 1.1 mg mL^{-1} in H_2O to 0.20 mg mL^{-1} in phosphate buffered saline (pH 7.2). UV–vis titrations of **12l** were not suitable for pK_a determination because changes of the absorption above pH 6 were quite small and depended strongly on experimental conditions (Figures S21, S22, Supporting Information). For [Ru(*p*-cymene)(bpy)(H_2O)]$^{2+}$ (bpy = 2,2′-bipyridine), a pK_a value for coordinated H_2O of 7.2 was reported,[48] for the osmium analogue [Os(*p*-cymene)(bpy)-(H_2O)]$^{2+}$, pK_a = 5.8 was found.[49] Therefore an overlapping of the deprotonation steps at the quinoxalinone and the aqua ligands is at least conceivable for **12l**.

X-ray Crystallography. The results of the X-ray diffraction studies of three ligands and six metal complexes are shown in Figures 8–10 and S22–S36 of the Supporting Information. A

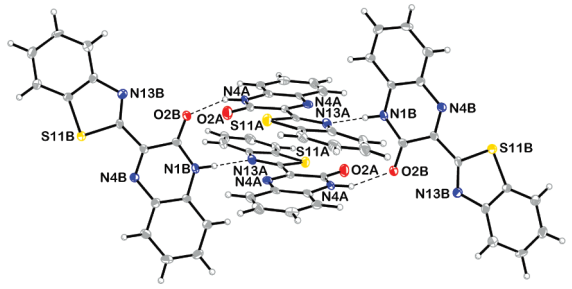

Figure 8. Associates of **4l** formed by hydrogen bonds; thermal ellipsoids are drawn at 40% probability level. Dashed lines represent hydrogen bonds.

more detailed discussion of the crystal structures is given in the Supporting Information.

The unsubstituted benzazolylquinoxalinone ligands crystallized in the monoclinic space groups *C*2/*c* (**4a**) or *P*2$_1$/*c* (**4h**, **4l**). In each case, the asymmetric unit consists of two molecules, which mainly differ by the twist angle between the quinoxalinone and the benzazole moiety ranging from 1.7° to 4.6° for the first and from 7.3° to 12.2° for the second molecule. Thereby **4h** shows the smallest and **4a** the largest distortion from planarity. A three-dimensional network of hydrogen bonds in **4a** is presumably responsible for its poor solubility in many solvents (Figure S23, Supporting Information). H-Bond stabilized chains and tetrameric assemblies are observed in the crystal structures of **4h** and **4l**, correspondingly (Figures S25 and 8, Supporting Information).

dx.doi.org/10.1021/jm3000906 | J. Med. Chem. 2012, 55, 3398–3413

The organometallic compounds show the expected pseudo-octahedral "piano-stool" configuration (see Figure 9 for **8a** and Figure 10 for **9l**). The complexes are chiral due to the presence of the stereogenic metal center crystallizing as a racemic mixture of both enantiomers.

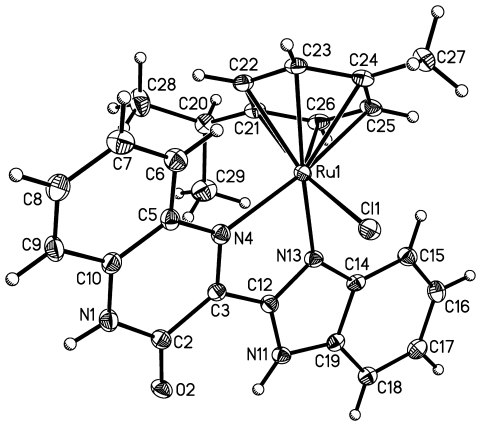

Figure 9. ORTEP plot of the complex cation of **8a** with atom numbering scheme. The thermal ellipsoids are drawn at 50% probability level. Selected bond lengths (Å) and bond angles (deg) for **8a**: Ru1−Cent^{cy} 1.7005(11), av Ru1−C^{cy} 2.21(3), Ru1−N4 2.145(2), Ru1−N13 2.074(2), Ru1−Cl1 2.4137(8), av C^{cy}−C^{cy} 1.416(5), C10−N1 1.389(3), N1−C2 1.358(3), C2−O2 1.235(3), C2−C3 1.473(4), C3−N4 1.327(3), N4−C5 1.397(3), C3−C12 1.431(4), C19−N11 1.380(3), N11−C12 1.362(3), C12−N13 1.326(3), N13−C14 1.395(3) Å. Cent^{cy}−Ru1−Cl1 128.99(5)°, Cent^{cy}−Ru1−N4 133.39(7)°, Cent^{cy}−Ru1−N13 129.74(7)°, N4−Ru1−Cl1 85.13(7)°, N13−Ru1−Cl1 84.77(7)°, N13−Ru1−N4 76.00(8)°, C2−N1−C10 122.8(2)°, C3−N4−C5 117.6(2)°, N13−C12−N11 112.5(2)°, C12−N11−C19 106.5(2)°, $\Theta_{(N4-C3-C12-N13)}$ −2.5(4)°.

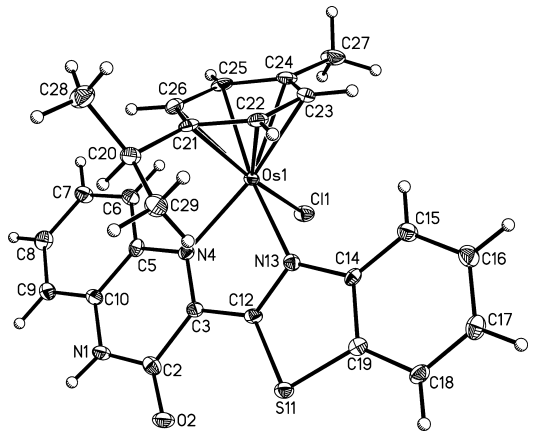

Figure 10. ORTEP plot of the complex cation of **9l** with atom numbering scheme. The thermal ellipsoids are drawn at 50% probability level. Selected bond lengths (Å) and bond angles (deg) for **9l**: Os1−Cent^{cy} 1.6959(14), av Os1−C^{cy} 2.21(3), Os1−N4 2.118(2), Os1−N13 2.101(2), Os1−Cl1 2.3951(7), av C^{cy}−C^{cy} 1.420(4), C10−N1 1.389(4), N1−C2 1.331(4), C2−O2 1.232(4), C2−C3 1.469(4), C3−N4 1.329(4), N4−C5 1.408(4), C3−C12 1.427(4), C19−S11 1.730(3), S11−C12 1.719(3), C12−N13 1.330(4), N13−C14 1.401(4) Å. Cent^{cy}−Os1−Cl1 129.47(5)°, Cent^{cy}−Os1−N4 130.87(8)°, Cent^{cy}−Os1−N13 130.70(7)°, N4−Os1−Cl1 84.90(7)°, N13−Os1−Cl1 86.35(7)°, N13−Os1−N4 76.20(9)°, C2−N1−C10 123.6(3)°, C3−N4−C5 117.0(3)°, N13−C12−S11 116.6(2)°, C12−S11−C19 88.69(14)°, $\Theta_{(N4-C3-C12-N13)}$ 1.3(4)°.

The ligands are always coordinated to the metal via the N4 of the quinoxalinone moiety and the atom N13 of the benzazole group.

Some average structural data concerning the coordination sphere are summarized in Table 1.

Table 1. Selected Average Bond Lengths and Bond Angles in 8a, 8h, 8l, 9a, 9h, and 9l (M = Ru or Os; C^{cy} = Carbon of the Aromatic *p*-Cymene Ring; Cent^{cy} = Centroid of the Six C^{cy})

average bond length [Å]		average bond angle [deg]	
M−Cl1	2.399(12)	Cl1−M−N4	86(1)
M−N4	2.126(13)	Cl1−M−N13	86(1)
M−N13	2.084(15)	N4−M−N13	76.0(4)
M−Cent^{cy}	1.695(4)	Cent^{cy}−M−Cl1	128(1)
M−C^{cy}	2.21(3)	Cent^{cy}−M−N4	132(2)
M−C22/C26[a]	2.18(7)	Cent^{cy}−M−N13	130.8(7)
M−C24[b]	2.251(12)		
C^{cy}−C^{cy}	1.419(7)		

[a]Average of the shortest M−C^{cy} bond. [b]Average of the longest M−C^{cy} bond.

A comparison of bond lengths in metal-free and coordinated quinoxalinone ligands revealed mere insignificant (within 3 σ) or just minor changes. The twist between the quinoxalinone and the benzazole moieties in the coordinated ligand is mainly dependent on the packing (see Supporting Information, pages 33−44), which is strongly affected by the content of cocrystallized water and correlates with the space group (*C*2/*c*: water free, 20.3(2)°; $P\bar{1}$: 2H$_2$O, 10.5(7)°). In general, no marked structural differences between the corresponding ruthenium and osmium complexes were observed. Structural similarity with the osmium analogues has already been noted for other organo-ruthenium compounds.[46]

Cytotoxicity in Cancer Cells. The cytotoxic potency of the quinoxalinone derivatives **4a**, **4h**, and **4l**, the ruthenium(II) (**8a**−**o**, **10a**) and osmium(II) complexes (**9a**, **9h**, **9l**) was determined in the human tumor cell lines A549 (nonsmall cell lung cancer), CH1 (ovarian carcinoma), and SW480 (colon carcinoma) by means of the colorimetric MTT assay.

In general, the CH1 cells were more sensitive to the compounds investigated in this study than the other cell lines. The IC$_{50}$ values of the three unsubstituted metal-free ligands (the substituted derivatives could not be tested for solubility reasons) vary within small ranges of micromolar concentrations in each cell line, whereas the potencies of the metal complexes vary within 2 orders of magnitude, with IC$_{50}$ values ranging from high nanomolar to medium micromolar concentrations, depending on the ligand substitutions and the metal ion (Table 2).

The following structure−activity relationships can be deduced from the cytotoxicity data: The quinoxalinone derivatives **4a** (with a benzimidazole moiety), **4h** (with benzoxazole), and **4l** (with benzothiazole) hardly differ in their cytotoxicity in CH1 and SW480 cells (IC$_{50}$: 6.7−8.6 μM and 14−23 μM, respectively). In A549 cells, **4a** (IC$_{50}$: 17 μM) is the most potent of these three compounds, while **4l** (IC$_{50}$: 61 μM) is the least potent in this cell line. Complexation to ruthenium or osmium bound to cymene results in more clear-cut differences, with a rank order of cytotoxicity in CH1 and

dx.doi.org/10.1021/jm3000906 | J. Med. Chem. 2012, 55, 3398−3413

Table 2. Cytotoxicity of Ligands (4a, 4h, 4l), Ruthenium(II) Complexes (8a−o, 10a), and Osmium(II) Complexes (9a, 9h, 9l) in Three Human Cancer Cell Lines

	IC_{50} (μM)[a]		
compd	A549	CH1	SW480
	Ligands		
4a	17 ± 2	8.6 ± 1.9	23 ± 4
4h	38 ± 7	7.5 ± 1.0	14 ± 3
4l	61 ± 15	6.7 ± 1.1	20 ± 3
	Ru(II) Complexes		
8a	17 ± 3	4.3 ± 1.2	5.3 ± 0.7
8b	3.9 ± 0.6	0.34 ± 0.11	2.3 ± 0.7
8c	13 ± 1	1.8 ± 0.4	4.5 ± 0.6
8d	5.4 ± 0.7	0.54 ± 0.18	1.8 ± 0.3
8e	11 ± 2	1.6 ± 0.7	2.6 ± 0.8
8f	4.1 ± 0.7	1.7 ± 0.2	3.4 ± 0.6
8g	3.8 ± 0.8	0.93 ± 0.12	1.6 ± 0.2
8h	28 ± 7	6.2 ± 1.8	9.0 ± 0.8
8i	56 ± 6	4.3 ± 0.7	14 ± 1
8j	56 ± 4	5.7 ± 1.1	19 ± 3
8k	14 ± 3	3.8 ± 0.5	8.0 ± 0.7
8l	22 ± 2	1.2 ± 0.4	2.2 ± 0.3
8m	12 ± 1	0.52 ± 0.10	1.7 ± 0.3
8n	7.8 ± 0.4	0.40 ± 0.03	1.0 ± 0.2
8o	3.9 ± 0.2	0.36 ± 0.06	1.0 ± 0.1
10a	140 ± 17	34 ± 11	40 ± 5
	Os(II) Complexes		
9a	3.0 ± 0.4	0.92 ± 0.29	4.7 ± 0.6
9h	37 ± 6	2.8 ± 0.7	12 ± 1
9l	2.3 ± 0.5	0.36 ± 0.02	0.91 ± 0.36

[a] 50% inhibitory concentrations in A549, CH1, and SW480 cells after exposure for 96 h in the MTT assay. Values are means ± standard deviations obtained from at least three independent experiments.

SW480 cells depending on the variable heterocyclic moiety as follows: benzothiazole > benzimidazole > benzoxazole; or **8l** (IC_{50}: 1.2 and 2.2 μM) > **8a** (IC_{50}: 4.3 and 5.3 μM) > **8h** (IC_{50}: 6.2 and 9.0 μM, respectively), and **9l** (IC_{50}: 0.36 and 0.91 μM) > **9a** (IC_{50}: 0.92 and 4.7 μM) > **9h** (IC_{50}: 2.8 and 12 μM, respectively). In A549 cells, the ruthenium complexes are rather similar in activity (IC_{50}: 17−28 μM), whereas the osmium compound **9h** (IC_{50}: 37 μM) is considerably less cytotoxic than **9a** (IC_{50}: 3.0 μM) and **9l** (IC_{50}: 2.3 μM). The generally lower cytotoxicity of the complexes containing benzoxazole derivatives may be explained by their lower thermodynamic and kinetic stability. As already mentioned, it was not possible to measure 2D-NMR spectra in d_6-DMSO due to fast decomposition, while those of the analogue complexes with benzothiazole and benzimidazole ligands did not pose such severe problems. Still, the presence of the indirubin pharmacophore, as in the benzimidazole derivatives, is not an essential prerequisite for cytotoxicity, and exchange of nitrogen for sulfur may even be advantageous from the mere aspect of in vitro potency.

A comparison of the uncomplexed quinoxalinone derivatives with benzimidazole (**4a**) or benzothiazole (**4l**), their ruthenium cymene complexes (**8a**, **8l**), and the osmium analogues (**9a**, **9l**) reveals that complexation with osmium results in a more pronounced and more consistent increase in cytotoxicity (5−27 times lower IC_{50} values) than complexation with ruthenium (equal to 9 times lower IC_{50} values). For the analogue benzoxazole-containing compounds (**4h**, **8h**, **9h**), differences in cytotoxicity are mostly small and there is no consistent tendency with regard to the effects of complexation. The ruthenium complex **10a** (IC_{50}: 34−140 μM), where cymene is replaced by η^6-bound benzene, is by an order of magnitude less active than the cymene-containing analogue **8a** (IC_{50}: 4.3−17 μM) and still considerably less active than noncoordinated **4a** (IC_{50}: 8.6−23 μM). In contrast to **8a**, which is stable in water for at least several weeks, **10a** decomposes within a few days in aqueous solution, forming an amorphous unidentified insoluble product. This precipitation may account for the observed reduction of biological activity.

Furthermore, the consequences of chloro and methyl substitutions at the quinoxalinone derivatives for the cytotoxic potency of the ruthenium complexes were studied. A comparison of the ruthenium complexes of benzimidazole and benzothiazole derivatives reveals a favorable effect of chloro substitutions, as chloro-only (**8b**, **8d**, **8n**) and mixed chloro/methyl substituted species (**8f**, **8g**, **8o**) are at least as potent as or more potent than the corresponding methyl-only substituted species (**8c**, **8e**, **8m**), which in turn are at least as potent as complexes **8a** and **8l** with unsubstituted ligands. For the complexes with benzoxazole ligands, the effects of methyl substituents are not consistent; only substitution in positions 6 and 7 (see atom numbering Scheme 1a) of the quinoxalinone moiety in complex **8k** is more likely to be advantageous. Complexes with chloro substituents at benzoxazole ligands could not be obtained in sufficient purity because these substituents further destabilize these generally not very robust compounds. Anyway, the partially somewhat higher cytotoxicities resulting from the substituents hardly outweigh the pronounced decrease of solubility with all its disadvantages for drug formulation and bioavailability.

Cell Cycle Perturbations. The impact of the lead structure indirubin-3′-monoxime as well as compounds **4a**, **8a**, **8h**, **8l**, **9a**, **9h**, and **9l** on cell cycle progression of exponentially growing A549 cells was studied by flow cytometry of propidium iodide-stained cells (Figure 11). Of these compounds, indirubin-3′-monoxime and the uncomplexed, unsubstituted quinoxalinone derivative **4a** have the most pronounced effects. In accordance with literature data,[25,50] indirubin-3′-monoxime induces a cell cycle arrest in G2/M phases. Similarly, **4a** induces a marked increase of the G2/M fraction, accompanied by a decrease of the G0/G1 and S fractions. The maximum effects of indirubin-3′-monoxime and **4a** were observed at concentrations of 40 and 160 μM, respectively, inducing increases of the G2/M fraction from 10% (in untreated controls) to 49% and 35%, respectively. Exposure to 40 μM **4a** for 24 h results in an increase of the G2/M fraction to 29%, which is about half the effect of indirubin-3′-monoxime, corresponding to their different cytotoxic potencies (IC_{50} values after 96 h: 17 and 7.9 μM,[51] respectively).

In contrast, the complexes **8a** and **9a** exert only marginal effects on the cell cycle despite their equal or even higher cytotoxicity. In particular, the apparent G2/M-arresting effect of **4a** is nearly completely abolished by complexation to ruthenium or osmium. The consequences of replacing the benzimidazole moiety of these complexes with benzoxazole or benzothiazole are moderate, with an increase of the G0/G1 fraction from 49 to 72% and a concomitant decrease of the S fraction from 37 to a minimum of 12% induced by 100 μM **8h** being the most conspicuous effect.

Induction of Apoptosis. The capacity of **8a**, **8l**, **9a**, and **9l** to induce apoptotic cell death was verified in a qualitative manner by fluorescence microscopy of SW480 cells treated for

dx.doi.org/10.1021/jm3000906 | J. Med. Chem. 2012, 55, 3398−3413

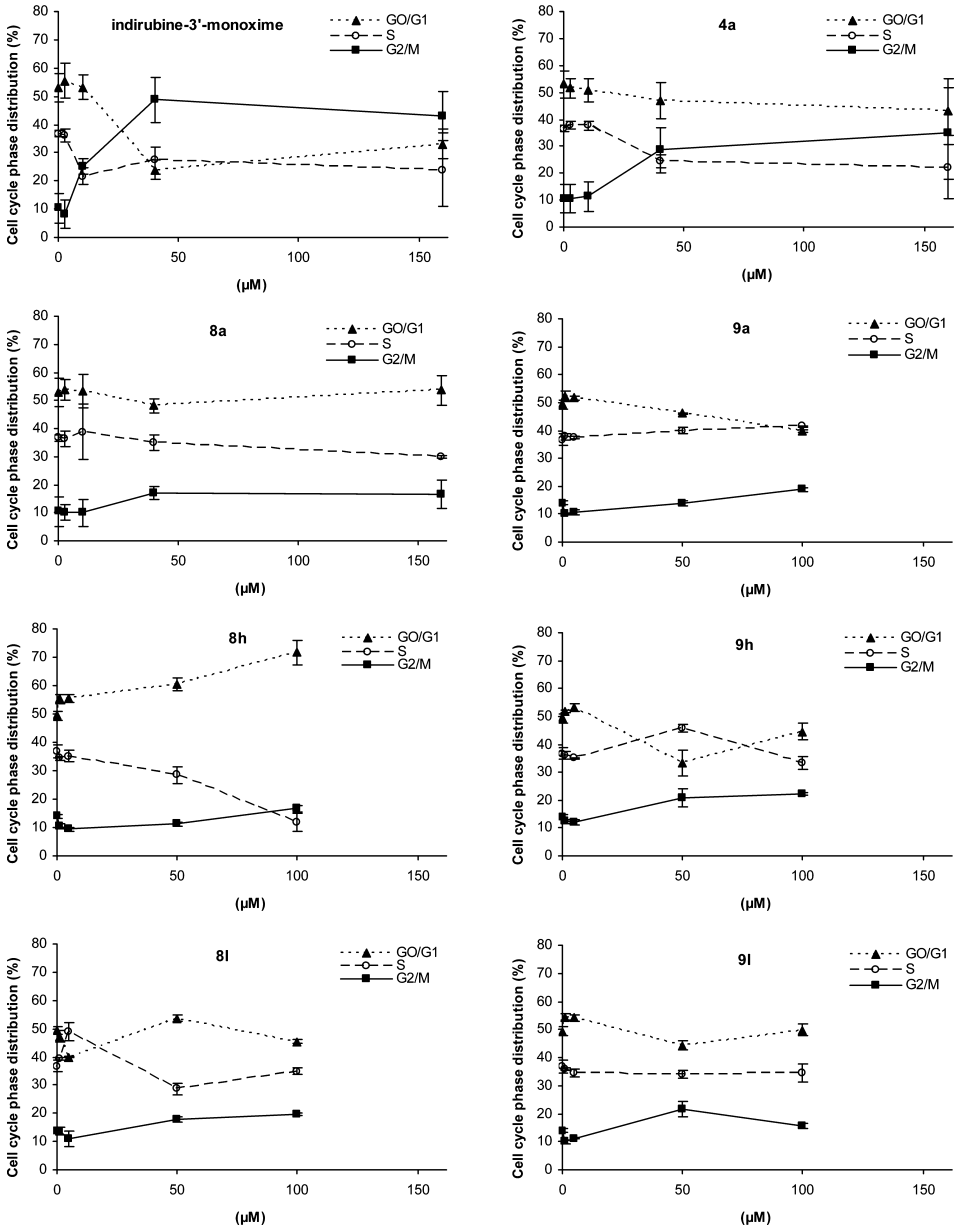

Figure 11. Concentration-dependent impact of indirubine-3′-monoxime, **4a**, **8a**, **8h**, **8l**, **9a**, **9h**, and **9l** on the cell cycle distribution of A549 cells after exposure for 24 h. Cells were analyzed for DNA content by flow cytometry after staining with propidium iodide.

24 h with low micromolar concentrations (1.25−10 μM) of the compounds and subsequently stained with DAPI. The microscopic images depicted in Figure 12 give clear evidence of the formation of apoptotic bodies, recognizable by the characteristic fragmentation of nuclei with bright condensed chromatin, for treatment with each of the compounds.

According to the flow-cytometric annexin V/propidium iodide assay, the ruthenium and osmium complexes with unsubstituted ligands derived from benzimidazole or benzothiazole are all capable of inducing apoptosis in SW480 colon cancer cells in a concentration-dependent manner, but with different potencies corresponding to their different cytotoxicities in the MTT assay (Figure 13). Variation of the heteroatom in the ligand has a more pronounced impact on the potencies of the compounds than the change of the central metal. At a concentration of 10 μM and within 48 h, complexes **8l** and **9l** with benzothiazole-derived ligands induce apoptosis in totals of about 67 and 43%, respectively, whereas the benzimidazole-based analogues **8a** and **9a** exert comparatively modest effects with totals of about 13 and 8%, respectively (Figure 14). However, especially at higher concentrations of the latter two compounds, apoptosis is accompanied by noteworthy fractions of necrotic cells (about 28 and 22% at 20 μM, respectively). Comparison of apoptosis-to-necrosis ratios reveals marked differences depending on the variable heteroatom in the ligand. Benzothiazole-derived compounds yield much higher ratios (**8l**: 10 μM, 4.7; 20 μM, 4.6. **9l**: 10 μM, 4.0; 20 μM, 6.3) than benzimidazole analogues (**8a**: 10 μM, 1.3; 20 μM, 0.64. **9a**: 10 μM, 2.9; 20 μM, 1.0). For a complete set of percentage values averaged from three independent experiment series, see Table S2 in the Supporting Information.

dx.doi.org/10.1021/jm3000906 | J. Med. Chem. 2012, 55, 3398−3413

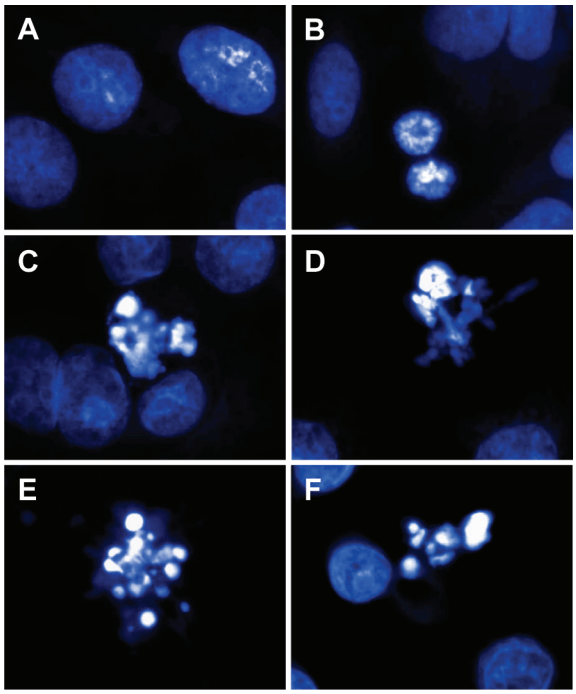

Figure 12. Formation of apoptotic bodies upon treatment of SW480 cells with quinoxalinone complexes: (A) untreated control; (B) untreated control with late mitotic nuclei; (C) **8a** (2.5 μM); (D) **8l** (5 μM); (E) **9a** (5 μM); (F) **9l** (1.25 μM).

CONCLUSIONS

A series of new ruthenium and osmium arene complexes containing quinoxalinone ligands with structural features that may contribute to specific interactions with biological targets has been prepared and tested for cytotoxicity in the three human cancer cell lines CH1 (ovarian carcinoma), SW480 (colon carcinoma), and A549 (nonsmall cell lung carcinoma). Comparison of structural aspects did not reveal significant differences between the two metals. The coordination of quinoxalinone derivatives to the metal results in a shift of the pK_a value for the lactam N–H from ca. 9 to 7. Thereby the solubility is impaired, but it is still much higher than that of the metal-free ligand. Complex **10a** containing a η^6-bound benzene seems to decompose with formation of an insoluble product, leading to IC_{50} values higher than those of the metal-free ligand. The lower activity of complexes with benzoxazole derivatives may also be due to diminished complex stability. The chlorido ligand is a potential leaving group that could provide a site for coordinative interaction with targets, with reactivity depending on the central ion. For the compounds presented herein, the higher inertness of osmium tends to be advantageous in terms of cytotoxicity in cancer cells. This might indicate that either coordination does not play any role in the mode of action or that the higher reactivity of ruthenium compounds results in deactivating side reactions. Evidently, effects on the cell cycle seem to be diminished by coordination to ruthenium or osmium, although cytotoxicity is enhanced or at least maintained and selected complexes all induce apoptosis in the low micromolar concentration range, suggesting that other effects not affecting the cell cycle contribute to their activity in vitro. All these findings should be taken into consideration for the future design of new enzyme-targeted metal-based drugs, which certainly open up new possibilities beyond the limitations of purely organic compounds.

EXPERIMENTAL SECTION

All solvents and reagents, if available in analytical grade, were purchased from commercial suppliers and used without further purification. Water from a reverse osmotic demineralization facility was distilled before use. Indirubin-3′-monoxime[25] and the precursors $[(\eta^6\text{-}p\text{-cymene})RuCl_2]_2$ (**7a**),[52,53] $[(\eta^6\text{-benzene})RuCl_2]_2$,[52] and $[(\eta^6\text{-}p\text{-cymene})OsCl_2]_2$ (**7b**)[54] were prepared according to literature protocols. $H_2[OsCl_6]$ was prepared by using hydrazine dihydrochloride for the reduction of osmium tetroxide in HCl.[55] In such a way, heating of the hazardous volatile OsO_4 was avoided. Elemental analyses of all biologically tested compounds were carried out on Carlo Erba (EA 1108 CHNS), Perkin-Elmer (2400 CHN), and Mettler-

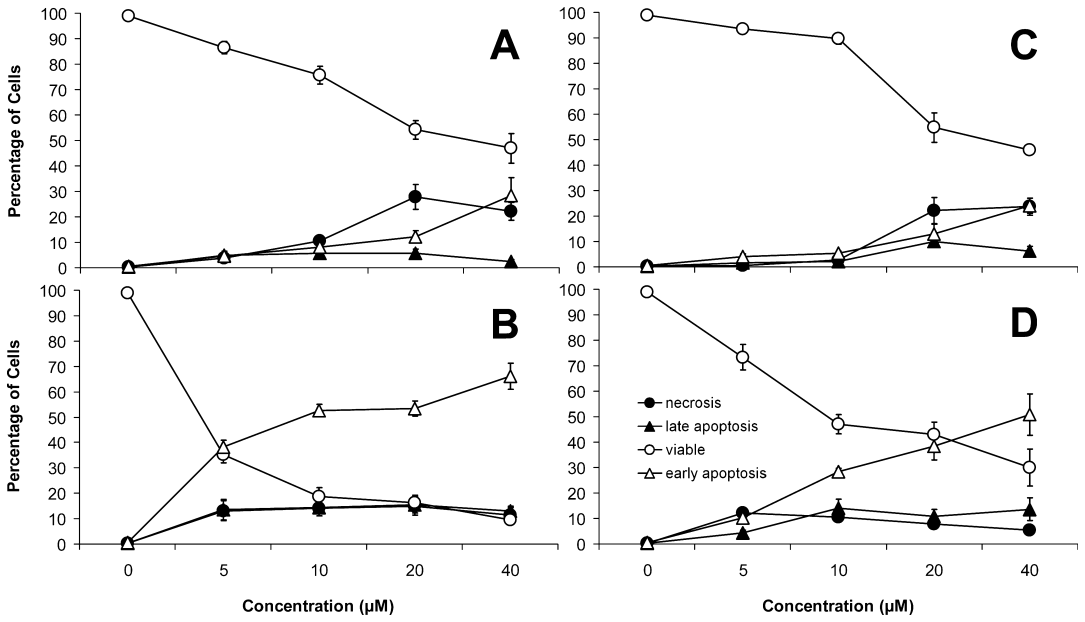

Figure 13. Percentages (means ± standard derivations) of viable, apoptotic, and necrotic SW480 cells after exposure to Ru and Os arene complexes with quinoxalinone ligands, **8a** (A), **8l** (B), **9a** (C), and **9l** (D) for 48 h, as obtained by flow cytometric quantification.

dx.doi.org/10.1021/jm3000906 | J. Med. Chem. 2012, 55, 3398–3413

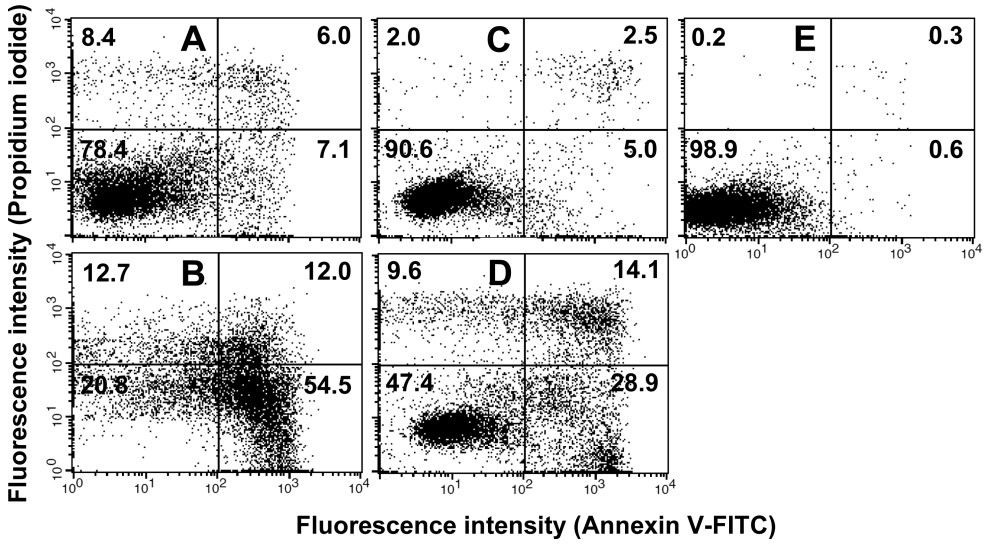

Figure 14. Flow cytometric quantification of viable, apoptotic, and necrotic SW480 cells after treatment with Ru and Os arene complexes with quinoxalinone ligands. Evaluation by annexin V-FITC versus propidium iodide staining of SW480 cells after 48 h incubation of 10 μM of compounds **8a** (A), **8l** (B), **9a** (C), and **9l** (D) compared to untreated control (E). Each bottom left quadrant contains viable, the bottom right early apoptotic, the top right late apoptotic and the top left necrotic cells (numbers indicate the respective percentages of total cell populations).

Toledo (DL 21) microanalyzers at the Microanalytical Laboratory of the University of Vienna and are within ±0.4%, confirming ≥95% purity, with exception of **10a**. An Esquire 3000 ion trap mass spectrometer (Bruker Daltonics, Bremen, Germany) with an orthogonal ESI ion source was used for MS measurements. The solutions in methanol were introduced via flow injection using a Cole-Parmer 74900 single-syringe infusion pump (Vernon Hills, IL). Expected and experimental isotope distributions were compared. Infrared spectra were obtained using a Bruker Vertex 70 instrument equipped with a Specac Golden Gate single reflection diamond ATR unit (4000−550 cm^{-1}). UV−vis spectra were recorded on a Perkin-Elmer Lambda 650 UV−vis spectrophotometer using samples dissolved in methanol (800−210 nm). For the description of shoulders, the wavelength of the appropriate local minimum of the first derivative absolute value was quoted. ^{1}H, ^{13}C, ^{1}H,^{1}H−COSY, ^{1}H,^{1}H-TOCSY, ^{1}H,^{1}H-ROESY, ^{1}H,^{13}C-HSQC, ^{1}H,^{13}C-HMBC, ^{1}H,^{13}C-HSQC-TOCSY, ^{1}H,^{15}N-HSQC, and ^{1}H,^{15}N-HMBC NMR spectra were recorded in DMSO-d_6, MeOH-d_4, or D_2O with a Bruker Avance III 500 MHz FT-NMR spectrometer. The 2D NMR spectra were measured in a gradient-enhanced mode. The residual ^{1}H and ^{13}C present in the solvents were used as internal references. ^{15}N shifts are quoted relative to external NH_4Cl. For the monitoring of the time-dependent interconversion between chlorido- and aqua-species, tetramethylammonium nitrate (0.13 mM) was used as internal reference. The automatically generated series of proton spectra were baseline corrected and integrated using AU programs included in Topspin 2.0 (Bruker Biospin Inc., Fremont, CA). The normalized peak areas were plotted against the time with Excel software (Microsoft Office Excel 2003, SP3, Microsoft Corporation). Abbreviation for NMR data: cy = *p*-cymene.

NMR Titrations. Complexes **11a**, **11h**, **11l**, **12a**, **12h**, or **12l** (3 mg) were dissolved in D_2O (0.6 mL) at ∼298 K. The pD value was measured directly in the NMR tubes with an Eco Scan pH6 pH meter equipped with a glass-micro combination pH electrode (Orion 9826BN), which was calibrated with standard buffer solutions of pH 4.00, 7.00, and 10.00. The pH titration was accomplished by addition of NaOD (0.4−0.0004% in D_2O) and DNO_3 (0.4−0.0004% in D_2O). The observed shifts of quinoxalinone ligand or cymene protons in the ^{1}H NMR spectra were plotted against the pD value with Excel software.

UV Titrations. The titrations were performed in a quartz cell, whereby the pH was measured with the pH electrode used for NMR titrations. Details are specified in the legends of the corresponding curves, created with Excel software by plotting the absorbance at a selected wavelength against the pH.

Crystallographic Structure Determinations. X-ray diffraction quality single crystals of the ligands **4a**, **4h**, and **4l** were obtained by slow diffusion of diethyl ether into their solutions in DMF. Single crystals of the corresponding ruthenium(II) complexes (**8h**, **8l**) and osmium(II) complexes (**9a**, **9h**, **9l**) were obtained by slow diffusion of sodium chloride into solutions of the compounds in water. Crystals of **8a** grew from D_2O solution during NMR measurements after addition of sodium chloride. Measurements were performed on a Bruker X8 APEXII CCD diffractometer at 100 K. Single crystals were positioned at 40 mm from the detector and measured under the following conditions: (**4a**) 1044 frames for 100 s over 1°, (**4h**) 2405 frames for 20 s over 1°, (**4l**) 1234 frames for 100 s over 1°, (**8a**) 931 frames for 20 s over 1°, (**8h**) 782 frames for 60 s over 1°, (**8l**) 1626 frames for 80 s over 1°, (**9a**) 2548 frames for 20 s over 1°, (**9h**) 1277 frames for 50 s over 1°, and (**9l**) 1395 frames for 50 s over 1°. The data were processed using the SAINT software package.[56] Crystal data, data collection parameters, and structure refinement details are given in Table S1, Supporting Information. The structures were solved by direct methods and refined by full-matrix least-squares techniques. Non-hydrogen atoms were refined with anisotropic displacement parameters. H atoms were inserted at calculated positions and refined with a riding model. The following computational resources were used: structure solution, SHELXS-97;[57] refinement, WinGX,[58] SHELXL-97;[59] calculations, PLATON;[60] molecular diagrams, XP 5.1 (Bruker, 1998);[61] computer, Pentium Dual Core; scattering factors.[62] Crystallographic data have been deposited with the Cambridge Crystallographic Data Center with the numbers CCDC 863692−863700. Copy of data can be obtained, free of charge, on application to The Cambridge Crystallographic Data Center, 12 Union Road, Cambridge CB2 1EZ, U.K. (deposit@ccdc.com.ac.uk).

Cell Lines and Culture Conditions.[42] CH1 cells originate from an ascites sample of a patient with a papillary cystadenocarcinoma of the ovary and were a generous gift from Lloyd R. Kelland, CRC Centre for Cancer Therapeutics, Institute of Cancer Research, Sutton, UK. SW480 (adenocarcinoma of the colon) and A549 (nonsmall cell lung cancer) cells were kindly provided by Brigitte Marian (Institute of Cancer Research, Department of Medicine I, Medical University of Vienna, Austria). All cell culture reagents were obtained from Sigma-Aldrich Austria. Cells were grown in 75 cm^2 culture flasks (Iwaki) as adherent monolayer cultures in Minimal Essential Medium (MEM) supplemented with 10% heat-inactivated fetal calf serum, 1 mM

dx.doi.org/10.1021/jm3000906 | J. Med. Chem. 2012, 55, 3398−3413

sodium pyruvate, and 2 mM L-glutamine. Cultures were maintained at 37 °C in a humidified atmosphere containing 5% CO_2 and 95% air.

Cytotoxicity in Cancer Cell Lines. Cytotoxicity in the cell lines mentioned above was determined by the colorimetric MTT (3-(4,5-dimethyl-2-thiazolyl)-2,5-diphenyl-2*H*-tetrazolium bromide, purchased from Sigma-Aldrich) microculture assay,[63] with modifications as described previously.[42] For this purpose, cells were harvested from culture flasks by trypsinization and seeded in 100 μL aliquots into 96-well microculture plates (Iwaki/Asahi Technoglass). Cell densities of 1.5×10^3 cells/well (CH1), 2.5×10^3 cells/well (SW480), and 4×10^3 cells/well (A549) were chosen in order to ensure exponential growth of untreated controls throughout drug exposure. Cells were allowed to settle and resume proliferation in drug-free complete culture medium for 24 h. The not sufficiently water-soluble test compounds were dissolved in DMSO and diluted in complete culture medium such that the maximum DMSO content did not exceed 0.5% (especially in the case of **4a**, **4h**, and **4l**, this procedure yielded opaque but colloidal solutions from which no precipitates could be separated by centrifugation). Only **8h−k**, **9h**, and **10a** were directly dissolved in medium under sonication. Appropriate dilutions were added in 100 μL aliquots to the microcultures, and cells were exposed to the test compounds for 96 h. At the end of exposure, all media were replaced by 100 μL/well RPMI1640 culture medium (supplemented with 10% heat-inactivated fetal bovine serum and 4 mM L-glutamine) plus 20 μL/well MTT (5 mg/mL) dissolved in phosphate-buffered saline (PBS). After incubation for 4 h, the supernatants were removed and the formazan crystals formed by viable cells were dissolved in 150 μL of DMSO per well. Optical densities at 550 nm were measured with a microplate reader (Tecan Spectra Classic), using a reference wavelength of 690 nm to correct for unspecific absorption. The quantity of viable cells was expressed as percentage of untreated controls, and 50% inhibitory concentrations (IC_{50}) were calculated from concentration−effect curves by interpolation. Evaluation is based on means from at least three independent experiments, each comprising three replicates per concentration level.

Cell Cycle Analyses. A549 cells (1×10^6 cells) were seeded into Petri dishes and allowed to recover for 24 h. Cells were then exposed for 24 h to the test compounds, dissolved as described for the MTT assays. Control and treated cells were collected, washed with PBS, fixed in 70% ice-cold ethanol, and stored at −20 °C. To determine cell cycle distributions, cells were transferred in physiological NaCl solution into PBS, incubated with 10 μg/mL RNase A for 30 min at 37 °C, and treated with 5 μg/mL propidium iodide for 30 min, and their fluorescence was measured by flow cytometry, using a FACS Calibur instrument (Becton Dickinson, Palo Alto, CA). The resulting DNA histograms were analyzed by Cell Quest Pro software (Becton Dickinson and Company, New York, USA).

Fluorescence Microscopy. Induction of apoptosis in SW480 was verified by fluorescence microscopy after DAPI staining. For this purpose, 2.5×10^5 cells/well were seeded in culture medium onto cover glasses in 6-well plates and allowed to attach for 24 h at 37 °C. Cells were then exposed to various concentrations of the test compounds for 24 h. The supernatant was removed, and cells were treated for 15 min with 1 μg/mL DAPI (4′,6-diamidino-2-phenylindole) in methanol. After washing the cells with methanol, the cover glasses were mounted on microscopy slides with mounting medium. Fluorescence images were taken on an Olympus BX-40 microscope using an excitation wavelength of 345 nm.

Annexin V/Propidium Iodide Assay. This assay was applied to determine the capacity of inducing cell death of the compounds under investigation. The method was described by Aubry et al.[64] and allows differentiation of early and late apoptosis as well as necrosis. In early apoptosis, phosphatidylserine flips from the inner side of the plasma membrane to the cell surface. The Ca^{2+}-dependent affinity of phosphatidylserine to an annexin V-FITC conjugate enables the fluorometric detection of this process by stimulation at a wavelength of 488 nm, resulting in emission at a wavelength of 530 nm. Staining with propidium iodide (PI), having an absorption wavelength of 990 nm and an emission wavelength of 612 nm, on the other hand, requires a loss of cell membrane integrity and therefore only works in the advanced apoptotic stage or in necrotic cells. For this purpose, 2×10^5 SW480 cells per well were seeded out in 6-well plates and allowed to recover for 24 h. Cells were then exposed to different concentrations of the test compounds for 48 h. The supernatant and cells detached by trypsinization were collected and transferred into FACS tubes, centrifuged at 1200 rpm for 3 min, and the supernatant was discarded. After resuspension in 0.5 mL of binding buffer, cells were incubated for 5 min with 1 μL of annexin V-FITC from Bio Vision. PI was added shortly before measurement in an effective concentration of 1 μg/mL. Fluorescence of 10000 cells was measured by flow cytometry with a FACS Calibur instrument (Becton Dickinson, Franklin Lakes, NJ) using FL1 channel for annexin V-FITC and FL2 channel for PI staining. Resulting dot blots were quantified by Cell Quest Pro software (Becton Dickinson and Company, Franklin Lakes, NJ).

Synthesis of Ligands and Metal Complexes. Microanalytical data, mass spectrometry, IR- and UV−vis-, ^1H and ^{13}C NMR spectra for all biologically tested compounds can be found in Supporting Information, along with the syntheses of precursors.

General Procedure A. A mixture of ethyl 2-(1*H*-benzimidazol-2-yl)-2,2-dibromoacetate or a substituted derivative (1 equiv), 1,2-phenylenediamine or a substituted derivative (1.1−1.4 equiv), and sodium acetate (3 equiv) in ethanol (96%, 7−8 mL/mmol) was sonicated until the starting compounds were dissolved at room temperature. In some cases, a yellow product started to precipitate prior the complete dissolution of starting material so that there was never a clear (red) solution. Subsequently, the reaction mixture was refluxed under argon (to avoid formation of oxidation side products from excess phenylendiamine) for 60 min. Afterward, the formed suspension was cooled and stored in a freezer (−20 °C) for 2−3 h. The solid was filtered off by suction and washed with cold ethanol (1−2 mL/mmol), water (4−5 × 2−4 mL/mmol), methanol (2 × 1−2 mL/mmol), and diethyl ether (3 × 3−4 mL/mmol). Finally, the crude product was dried in vacuo.

*3-(1H-Benzimidazol-2-yl)-1H-quinoxalin-2-one (**4a**).* The reaction was performed according to procedure A using **3a** (5.47 g, 15.0 mmol) and 1,2-phenylenediamine (2.22 g, 20.0 mmol). The crude product was dissolved in acetic acid (45 mL) and precipitated by addition of diethyl ether (100 mL). The solid was filtered off, washed with diethyl ether (3 × 25 mL), and dried in vacuo. Then the material was suspended in water (100 mL) and dissolved by addition of orthophosphoric acid (85%, 5.1 mL, 75 mmol). The solution was filtered and the filtrate poured into a solution of sodium hydroxide (4.59 g, 113 mmol) in water (100 mL). After cooling (+2 °C) for 1 h, the precipitate was filtered off and washed with water (3 × 70 mL). The solid was suspended in water (100 mL), heated to 100 °C for 30 min, filtered off again, and washed with water (2 × 70 mL). Finally, the product was dried in vacuo. Yield: 3.18 g (80%). Anal. ($C_{15}H_{10}N_4O$): C, H, N. Alternatively, the compound was synthesized by reaction of ethyl 3-oxo-3,4-dihydro-quinoxaline-2-carboxylate[65] (0.22 g, 1.0 mmol) and 1,2-phenylenediamine (0.13 g, 1.2 mmol) in ethylene glycol (4.0 mL) under argon at 170 °C for 3 h. After cooling to room temperature, the mixture was allowed to stand in a freezer (−20 °C) for 3−4 h. Then the crude product was filtered off by suction, washed with methanol (3 × 3 mL), and dried in vacuo. The purification was performed as described above using acetic acid (3.5 mL), diethyl ether (8 mL, 3 × 5 mL), 1 M aqueous orthophosphoric acid (4 mL), 1 M aqueous sodium hydroxide (4.5 mL), and water (5 × 10 mL). Yield: 0.09 g (34%).

*3-(5,6-Dichloro-1H-benzimidazol-2-yl)-1H-quinoxalin-2-one (**4b**).* The reaction was performed by following procedure A, but reducing the reaction time to 10 min, starting from **3b** (1.51 g, 3.5 mmol) and 1,2-phenylenediamine (0.52 g, 4.7 mmol). Yield: 1.03 g (88%). The crude product was used for complexation reactions without further purification.

*3-(5,6-Dimethyl-1H-benzimidazol-2-yl)-1H-quinoxalin-2-one (**4c**).* **3c** (0.82 g, 2.1 mmol) and 1,2-phenylenediamine (0.32 g, 2.8 mmol) were refluxed in absolute methanol (20 mL) under argon for 30 min. Then 4-methylmorpholine (0.53 mL, 4.7 mmol) was added. Subsequently, the reaction mixture was refluxed for further 3 h. After cooling to 50 °C, the precipitate was filtered off by suction and washed

with methanol (2 × 7 mL), water (5 × 10 mL), methanol (2 × 7 mL), and diethyl ether (3 × 10 mL). The crude product was recrystallized from ethylene glycol (60 mL), filtered off, washed with methanol (3 × 8 mL), and dried in vacuo. Yield: 0.27 g (43%).

*3-(1H-Benzimidazol-2-yl)-6,7-dichloro-1H-quinoxalin-2-one (**4d**).* The reaction was performed according to procedure A starting from **3a** (1.09 g, 3.0 mmol) and 4,5-dichloro-1,2-phenylenediamine (0.73 g, 4.0 mmol). Yield: 0.94 g (94%). The crude product was used for complexation without further purification.

*3-(1H-Benzimidazol-2-yl)-6,7-dimethyl-1H-quinoxalin-2-one (**4e**).* 4,5-Dimethyl-1,2-phenylenediamine (0.46 g, 3.3 mmol) and sodium acetate (0.83 g, 10 mmol) were dissolved in a mixture of ethanol (96%, 20 mL) and water (1 mL). Activated charcoal was added, and the resulting suspension was stirred at room temperature for 40 min. Subsequently, the charcoal was removed by filtration through a small column with silica (3 g). To the filtrate, **3a** (1.09 g, 3.0 mmol) was added as a solid and the reaction mixture immediately sonicated until the starting compound had dissolved. Subsequently, the flask was closed under argon and allowed to stand at room temperature for 2 h. Then the formed solid was filtered off by suction and washed with ethanol (10 mL), water (4 × 15 mL), ethanol (2 × 10 mL), and diethyl ether (3 × 15 mL). Finally, the product was dried in vacuo. Yield: 0.84 g (96%).

*3-(5,6-Dichloro-1H-benzimidazol-2-yl)-6,7-dimethyl-1H-quinoxalin-2-one (**4f**).* The reaction was performed according to procedure A, applying a longer refluxing time (1.5 h), starting from **3b** (2.16 g, 5.0 mmol) and 4,5-dimethyl-1,2-phenylenediamine (0.97 g, 7.0 mmol). The crude product was suspended in water (100 mL), heated to 100 °C for 1 h, filtered off, and washed with water (3 × 15 mL). Finally, the product was dried in vacuo. Yield: 1.68 g (70%).

*6,7-Dichloro-3-(5,6-dimethyl-1H-benzimidazol-2-yl)-1H-quinoxalin-2-one (**4g**).* The compound was prepared as described above for **4e** starting from 4,5-dichloro-1,2-phenylenediamine (0.37 g, 2.0 mmol), sodium acetate (0.39 g, 4.7 mmol), and **3c** (0.57 g, 1.46 mmol). The amounts of all solvents used were reduced to the half compared to those used for the synthesis of **4e**. Yield: 0.43 g (82%).

*3-(Benzoxazol-2-yl)-1H-quinoxalin-2-one (**4h**).* **3d** (2.55 g, 7.0 mmol) and 1,2-phenylenediamine (1.03 g, 9.3 mmol) were stirred in absolute methanol (50 mL) under argon at 50 °C for 30 min. Then 4-methylmorpholine (0.53 mL, 4.7 mmol) was added and the reaction mixture was stirred for further 5.5 h at 50 °C. After cooling to 5 °C, the precipitate was filtered off by suction, washed with cold methanol (2 × 7 mL), diethyl ether (4 × 15 mL), water (5 × 15 mL), methanol (5 mL), and diethyl ether (3 × 15 mL). The crude product was recrystallized from ethylene glycol (40 mL), filtered off, washed with methanol (3 × 8 mL), and dried in vacuo. To remove all ethylene glycol, the substance was dissolved in boiling methanol (450 mL). After cooling to room temperature, the solvent was evaporated at reduced pressure to $^1/_3$ of the initial volume. The suspension was chilled in a freezer (−20 °C) for 4 h before the precipitate was filtered off by suction, washed with cold methanol (10 mL), and dried in vacuo at 120 °C. Yield: 0.55 g (30%). Anal. ($C_{15}H_9N_3O_2$): C, H, N.

*3-(5-Methylbenzoxazol-2-yl)-1H-quinoxalin-2-one (**4i**).* To a solution of **3e** (10.3 g 27.3 mmol) in ethanol (96%, 50 mL) was added a solution of 1,2-phenylendiamine (3.98 g, 36 mmol) and sodium acetate (6.76 g, 81 mmol) in a mixture of ethanol (45 mL) and water (25 mL). The red solution formed was allowed to stand under argon and light protection at room temperature for 20 h. The precipitate was filtered off by suction and washed with ethanol (2 × 10 mL), water (4 × 25 mL), ethanol (10 mL), and diethyl ether (3 × 25 mL). The product was dried in vacuo and used without further purification in the next step. Yield: 4.78 g (63%).

*3-(6-Methylbenzoxazol-2-yl)-1H-quinoxalin-2-one (**4j**).* **3f** (4.53 g, 12 mmol), 1,2-phenylenediamine (1.77 g, 16 mmol), and sodium acetate (2.09 g, 25 mmol) were dissolved in a mixture of ethanol (96%, 40 mL) and water (10 mL). After 30 min sonication, the reaction mixture was stirred under argon and light protection at room temperature for 70 h. The solid was filtered off by suction and washed with ethanol (2 × 12 mL), water (3 × 15 mL), ethanol (10 mL), and diethyl ether (3 × 12 mL). The dried crude product was recrystallized three times from ethanol (3 × 320 mL). The product was dried in vacuo. Yield: 1.40 g (37%).

*3-(Benzoxazol-2-yl)-6,7-dimethyl-1H-quinoxalin-2-one (**4k**).* A suspension of **3d** (2.65 g, 7.3 mmol), 4,5-dimethyl-1,2-phenylendiamine (1.33 g, 9.7 mmol), and sodium acetate (1.84 g, 22 mmol) in ethanol (96%, 25 mL) was sonicated at 30 °C for 5 min before water (7.0 mL) was added and the sonication continued for additional 5 min. Subsequently, the reaction mixture was allowed to stand at 30 °C for further 3.5 h. The precipitate formed was filtered off by suction and washed with ethanol (2 × 15 mL), water (4 × 30 mL), ethanol (15 mL), and diethyl ether (4 × 30 mL). The product was dried in vacuo and used without further purification in the next step. Yield: 0.93 g (44%).

*3-Benzothiazol-2-yl-1H-quinoxalin-2-one (**4l**).* To a suspension of **6a** (4.74 g, 25 mmol) in ethanol (96%, 150 mL) was added 2-aminothiophenol (3.0 mL, 28 mmol). The mixture was refluxed under argon for 30 min. After the addition of hydrochloric acid (37%, 2.9 mL, 35 mmol), refluxing was continued for 2.5 h. Subsequently, the reaction mixture was cooled with an ice bath for 1 h. The yellow solid was filtered off and washed with cold ethanol (10 mL), water (5 × 12 mL), cold ethanol (5 mL), and diethyl ether (3 × 12 mL). The crude material was dissolved in a mixture of ethanol (750 mL) and tetrahydrofuran (150 mL) at 70 °C, filtered, and the filtrate poured into water (3500 mL). The precipitate was filtered off and washed with water (3 × 12 mL), cold ethanol (5 mL), and diethyl ether (2 × 12 mL). The dried substance was recrystallized from *o*-xylene (1000 mL). Thereby insoluble material was removed by hot filtration. After drying in vacuo at 80 °C, the yellow powder was dissolved in THF (2500 mL), filtered, and poured into water (10000 mL). The precipitate was filtered off by suction, washed with water (3 × 50 mL), and dried in vacuo at 70 °C. Yield: 1.90 g (27%). Anal. ($C_{15}H_9N_3OS$): C, H, N, S.

*3-(Benzothiazol-2-yl)-6,7-dimethyl-1H-quinoxalin-2-one (**4m**).* To a suspension of **6b** (0.87 g, 4.0 mmol) in ethanol (96%, 50 mL) was added 2-aminothiophenol (0.48 mL, 4.4 mmol). The mixture was refluxed under argon for 45 min. After the addition of hydrochloric acid (37%, 0.42 mL, 5 mmol), refluxing was continued for 3 h. The reaction mixture was allowed to cool to ca. 40 °C. The precipitate was filtered off by suction and washed with ethanol (2 × 5 mL). The crude material was refluxed in ethanol (50 mL) for 2.5 h. Subsequently, water (30 mL) was added and the boiling was continued for 1 h. The suspension was cooled to ca. 40 °C. The solid was filtered off and washed with water (3 × 15 mL), ethanol (5 mL), and diethyl ether (3 × 15 mL). Finally, the product was dried in vacuo and used for complexation without further purification. Yield: 0.74 g (60%).

*3-(5-Chlorobenzothiazol-2-yl)-1H-quinoxalin-2-one (**4n**).* To a suspension of **6a** (0.57 g, 3.0 mmol) in ethanol (96%, 30 mL) was added 2-amino-4-chloro-thiophenol (0.55 g, 3.3 mmol). The mixture was refluxed under argon for 45 min. After the addition of hydrochloric acid (37%, 0.42 mL, 5 mmol), refluxing was continued for 5.5 h. Subsequently, the reaction mixture was cooled with an ice bath for 15 min. The yellow solid was filtered off and washed quickly with cold ethanol (3 × 5 mL), water (5 × 15 mL), cold ethanol (5 mL), and diethyl ether (3 × 10 mL). Finally, the product was dried in vacuo and used for complexation without further purification. Yield: 0.72 g (76%).

*3-(5-Chlorobenzothiazol-2-yl)-6,7-dimethyl-1H-quinoxalin-2-one (**4o**).* **6b** (0.87 g, 4.0 mmol) and 2-amino-4-chloro-thiophenol (0.73 g, 4.4 mmol) were suspended in ethanol (96%, 40 mL) and refluxed for 75 min. Then hydrochloric acid (37%, 0.59 mL, 7 mmol) was added, and refluxing continued for 18 h. After cooling to ca. 50 °C, the crude product was filtered off by suction and washed with ethanol (2 × 10 mL) and water (4 × 15 mL). Subsequently, the orange material was suspended in water (40 mL) and refluxed under oxygen atmosphere for 2.5 h. Then the yellow solid was filtered off from the hot suspension and washed with boiling water (3 × 15 mL). Finally, the product was dried in vacuo over phosphorus pentoxide and used for complexation without further purification. Yield: 1.06 g (77%).

General Procedure B. A mixture of the quinoxalinone-ligand (1 equiv) and **7a** or **7b** (0.5 equiv) in absolute ethanol (7 mL/mmol ligand) was stirred at 70 °C for 45 min. Then hydrochloric acid (37%,

0.25 equiv) was added and stirring at 70 °C continued for further 7 h. Subsequently, the mixture was cooled and allowed to stand in a freezer (−20 °C) overnight. The precipitate was filtered off by suction and washed with diethyl ether (4 × 15 mL/mmol ligand). The crude product was dried in vacuo, dissolved in hydrochloric acid (10 mM, varying amounts), the solution filtered to remove solid impurities, the filtrate immediately frozen, and then lyophilized.

General Procedure C. A mixture of the quinoxalinone-ligand (1 equiv) and **7a** or **7b** (0.5 equiv) in absolute ethanol (8 mL/mmol ligand) was stirred at 70 °C for 45 min. After the addition of hydrochloric acid (37%, 0.25 equiv), stirring at 70 °C was continued for a further 5.5 h. The mixture was cooled to −20 °C, and absolute diethyl ether (varying amounts) was added under vigorous stirring. The suspension was allowed to stand at −20 °C for 1 h before the precipitate was filtered off by suction and washed with diethyl ether (4 × 15 mL/mmol ligand). The crude product was dried in vacuo, dissolved in hydrochloric acid (10 mM, varying amounts), and the solution filtered. The filtrate was immediately frozen and lyophilized.

*T-4-R/S-[3-(1H-Benzimidazol-2-yl-κN$^{3'}$)-1H-quinoxalin-2-one-κN^{4}]-chlorido-(η^{6}-1-isopropyl-4-methylbenzene)-ruthenium(II) Chloride (**8a**).* To a suspension of **4a** (0.26 g, 1.0 mmol) in absolute ethanol (10 mL) was added **7a** (0.25 g, 0.5 mmol). The mixture was stirred at room temperature for 15 min. Then the turbid dark-red solution was filtered. After the addition of absolute ethanol (5 mL) and diisopropyl ether (20 mL), the mixture was refluxed for 15 min and allowed to cool to room temperature. Subsequently, the reaction mixture was placed in a freezer overnight. The solid formed was filtered off by suction and washed with diethyl ether (3 × 12 mL). After drying, the crude product was dissolved in water (60 mL) and the solution filtered. The filtrate was immediately frozen and lyophilized. Yield: 0.28 g (45%). Anal. ($C_{25}H_{24}Cl_2N_4ORu·2H_2O$): C, H, N, Cl.

*T-4-R/S-Chlorido-[3-(5,6-dichloro-1H-benzimidazol-2-yl-κN$^{3'}$)-1H-quinoxalin-2-one-κN^{4}]-(η^{6}-1-isopropyl-4-methylbenzene)-ruthenium(II) Chloride (**8b**).* A mixture of **4b** (0.34 g, 1.0 mmol) and **7a** (0.31 g, 0.5 mmol) in absolute ethanol (10 mL) was allowed to stir at room temperature for 30 min. Then the mixture was heated to boiling and immediately filtered. Addition of diethyl ether to the cooled filtrate resulted in precipitation of the product, which was filtered off and washed with diethyl ether (3 × 12 mL). The crude solid was dissolved in dichloromethane (80 mL), the solution filtered, and the product precipitated again by addition of diethyl ether (150 mL). After washing with diethyl ether (25 mL) and drying in vacuo, the substance was dissolved in hydrochloric acid (10 mM, 80 mL) and the solution filtered. The filtrate was immediately frozen, and lyophilized. Yield: 0.25 g (57%). Anal. ($C_{25}H_{22}Cl_4N_4ORu·2H_2O$): C, H, N, Cl.

*T-4-R/S-Chlorido-[3-(5,6-dimethyl-1H-benzimidazol-2-yl-κN$^{3'}$)1H-quinoxalin-2-one-κN^{4}]-(η^{6}-1-isopropyl-4-methylbenzene)-ruthenium(II) Chloride (**8c**).* A mixture of the **4c** (0.20 g, 0.70 mmol) and **7a** (0.21 g, 0.35 mmol) in absolute ethanol (5 mL) was stirred at 70 °C for 30 min, forming a pulp. After the addition hydrochloric acid (37%, 0.009 mL, 0.1 mmol), stirring at 70 °C was continued for 8.5 h. To reduce the viscosity, the pulp was sonicated and shaken from time to time. Subsequently, the thick suspension was cooled and allowed to stand in the refrigerator at 2 °C for 4 h. The solid was filtered off and washed with absolute ethanol (3 mL) and diethyl ether (4 × 10 mL). The crude product was dried in vacuo, dissolved in water (220 mL), and the solution filtered. The filtrate was immediately frozen, and lyophilized. This purification step was repeated using water (100 mL). Yield: 0.25 g (57%). Anal. ($C_{27}H_{28}Cl_2N_4ORu·0.7H_2O$): C, H, N, Cl.

*T-4-R/S-[3-(1H-Benzimidazol-2-yl-κN$^{3'}$)-6,7-dichloro-1H-quinoxalin-2-one-κN^{4}]-chlorido-(η^{6}-1-isopropyl-4-methylbenzene)-ruthenium(II) Chloride (**8d**).* A mixture of **4d** (0.33 g, 1.0 mmol) and **7a** (0.31 g, 0.5 mmol) in absolute ethanol (10 mL) was allowed to stir at room temperature for 30 min and then heated to 70 °C for 10 min. When cooled to room temperature, activated charcoal (0.05 g) was added, whereupon the mixture was stirred at room temperature for 90 min. Then the charcoal was removed by filtration through a small column with cellulose powder (1.5 g). The filtrate was concentrated to 2.5 mL under reduced pressure, and under sonication diethyl ether (25 mL) was added. The precipitate was filtered off and washed with diethyl ether (3 × 7 mL). The crude material was treated with dichloromethane (60 mL), the solution was separated from undissolved material by filtration, and the filtrate was poured into diethyl ether (170 mL). The solid formed was filtered off, washed with diethyl ether (10 mL), and dried in vacuo. The substance was dissolved in hydrochloric acid (10 mM, 120 mL) and the solution filtered. The filtrate was immediately frozen, and lyophilized. Yield: 0.26 g (38%). Anal. ($C_{25}H_{22}Cl_4N_4ORu·2.5H_2O$): C, H, N, Cl.

*T-4-R/S-[3-(1H-Benzimidazol-2-yl-κN$^{3'}$)-6,7-dimethyl-1H-quinoxalin-2-one-κN^{4}]-chlorido-(η^{6}-1-isopropyl-4-methylbenzene)-ruthenium(II) Chloride (**8e**).* A mixture of **4e** (0.12 g, 0.4 mmol) and **7a** (0.12 g, 0.2 mmol) in absolute ethanol (4 mL) was stirred at 70 °C for 1 h, allowed to cool to room temperature, and stirred for a further 1.5 h. Then dry diethyl ether (10 mL) was added under vigorous stirring. Then 20 min later, the precipitate was filtered off and washed with diethyl ether (3 × 10 mL). The crude product was dried in vacuo, dissolved in hydrochloric acid (10 mM, 80 mL), and the solution filtered. The filtrate was immediately frozen and lyophilized. Yield: 0.18 g (70%). Anal. ($C_{27}H_{28}Cl_2N_4ORu·2.5H_2O$): C, H, N, Cl.

*T-4-R/S-Chlorido-[3-(5,6-dichloro-1H-benzimidazol-2-yl-κN$^{3'}$)-6,7-dimethyl-1H-quinoxalin-2-one-κN^{4}]-(η^{6}-1-isopropyl-4-methylbenzene)-ruthenium(II) Chloride (**8f**).* The complex was prepared according to general procedure B starting from **4f** (0.29 g, 0.8 mmol) and **7a** (0.25 g, 0.4 mmol) and by using hydrochloric acid (10 mM, 150 mL) for lyophilization. Yield: 0.31 g (54%). Anal. ($C_{27}H_{26}Cl_4N_4ORu·2.5H_2O$): C, H, N, Cl.

*T-4-R/S-Chlorido-[6,7-dichloro-3-(5,6-dimethyl-1H-benzimidazol-2-yl-κN$^{3'}$)-1H-quinoxalin-2-one-κN^{4}]-(η^{6}-1-isopropyl-4-methylbenzene)-ruthenium(II) Chloride (**8g**).* A mixture of **4g** (0.15 g, 0.4 mmol) and **7a** (0.12 g, 0.2 mmol) in absolute ethanol (5 mL) was stirred under argon at 70 °C for 2.5 h. After cooling to room temperature, acetone (12 mL) was added. The solid was filtered off and washed with acetone (2 × 7 mL) and diethyl ether (3 × 10 mL). The dried crude material was dissolved in hydrochloric acid (10 mM, 120 mL) at 70 °C and insoluble impurities removed by filtration. The filtrate was frozen and lyophilized. Yield: 0.14 g (51%). Anal. ($C_{27}H_{26}Cl_4N_4ORu·H_2O$): C, H, N, Cl.

*T-4-R/S-[3-(Benzoxazol-2-yl-κN$^{3'}$)-1H-quinoxalin-2-one-κN^{4}]-chlorido-(η^{6}-1-isopropyl-4-methylbenzene)-ruthenium(II) Chloride (**8h**).* The complex was prepared according to general procedure B starting from **4h** (0.11 g, 0.4 mmol) and **7a** (0.12 g, 0.2 mmol) and by using hydrochloric acid (10 mM, 20 mL) for lyophilization. The complex was dissolved in water (20 mL), filtered, the filtrate immediately frozen, and lyophilized again. Yield: 0.15 g (62%). Anal. ($C_{25}H_{23}Cl_2N_3O_2Ru·2H_2O$): C, H, N, Cl.

*T-4-R/S-Chlorido-[3-(5-methylbenzoxazol-2-yl-κN$^{3'}$)-1H-quinoxalin-2-one-κN^{4}]-(η^{6}-1-isopropyl-4-methylbenzene)-ruthenium(II) Chloride (**8i**).* The complex was prepared according to procedure C starting from **4i** (0.17 g, 0.6 mmol) and **7a** (0.19 g, 0.3 mmol). Diethyl ether (10 mL) was used for precipitation and hydrochloric acid (10 mM, 50 mL) for lyophilization. Yield: 0.30 g (80%). Anal. ($C_{26}H_{25}Cl_2N_3O_2Ru·2H_2O$): C, H, N, Cl.

*T-4-R/S-Chlorido-[3-(6-methylbenzoxazol-2-yl-κN$^{3'}$)-1H-quinoxalin-2-one-κN^{4}]-(η^{6}-1-isopropyl-4-methylbenzene)-ruthenium(II) Chloride (**8j**).* The complex was prepared according to general procedure B starting from **4j** (0.22 g, 0.70 mmol) and **7a** (0.22 g, 0.35 mmol) and by using hydrochloric acid for lyophilization (10 mM, 40 mL). Yield: 0.37 g (84%). Anal. ($C_{26}H_{25}Cl_2N_3O_2Ru·2H_2O$): C, H, N, Cl.

*T-4-R/S-[3-(Benzoxazol-2-yl-κN$^{3'}$)-6,7-dimethyl-1H-quinoxalin-2-one-κN^{4}]-chlorido-(η^{6}-1-isopropyl-4-methylbenzene)-ruthenium(II) Chloride (**8k**).* The complex was prepared according to general procedure B starting from **4k** (0.18 g, 0.6 mmol) and **7a** (0.19 g, 0.3 mmol) and by using hydrochloric acid for lyophilization (10 mM, 100 mL). Yield: 0.32 g (77%). Anal. ($C_{27}H_{27}Cl_2N_3O_2Ru·3H_2O$): C, H, N, Cl.

*T-4-R/S-[3-(Benzothiazol-2-yl-κN$^{3'}$)-1H-quinoxalin-2-one-κN^{4}]-chlorido-(η^{6}-1-isopropyl-4-methylbenzene)-ruthenium(II) Chloride (**8l**).* The complex was prepared according to general procedure B starting from **4l** (0.11 g, 0.4 mmol) and **7a** (0.12 g, 0.2 mmol) and by

using hydrochloric acid for lyophilization (10 mM, 25 mL). Yield: 0.18 g (66%). Anal. ($C_{25}H_{23}Cl_2N_3ORuS·1.6H_2O$): C, H, N, S, Cl.

*T-4-R/S-[3-(Benzothiazol-2-yl-κN$^{3'}$)-6,7-dimethyl-1H-quinoxalin-2-one-κN^4]-chlorido-(η^6-1-isopropyl-4-methylbenzene)-ruthenium-(II) Chloride (**8m**).* The complex was prepared according to general procedure B starting from **4m** (0.12 g, 0.4 mmol) and **7a** (0.12 g, 0.2 mmol) and by using hydrochloric acid for lyophilization (10 mM, 400 mL). The lyophilizate was dissolved in dichloromethane (130 mL), insoluble impurities removed by filtration, and the filtrate evaporated to dryness under reduced pressure. The residue was dissolved in water (120 mL), filtered, the filtrate immediately frozen, and lyophilized again. Yield: 0.12 g (46%). Anal. ($C_{27}H_{27}Cl_2N_3ORuS·2H_2O$): C, H, N, S, Cl.

*T-4-R/S-Chlorido-[3-(5-chlorobenzothiazol-2-yl-κN$^{3'}$)-1H-quinoxalin-2-one-κN^4]-(η^6-1-isopropyl-4-methylbenzene)-ruthenium(II) Chloride (**8n**).* The complex was prepared according to general procedure B starting from **4n** (0.13 g, 0.4 mmol) and **7a** (0.12 g, 0.2 mmol) and by using hydrochloric acid for lyophilization (10 mM, 200 mL). Yield: 0.21 g (82%). Anal. ($C_{25}H_{22}Cl_3N_3ORuS·H_2O$): C, H, N, S, Cl.

*T-4-R/S-Chlorido-[3-(5-chlorobenzothiazol-2-yl-κN$^{3'}$)-6,7-dimethyl-1H-quinoxalin-2-one-κN^4]-(η6−1-isopropyl-4-methylbenzene)-ruthenium(II) Chloride (**8o**).* The complex was prepared according to general procedure B starting from **4o** (0.14 g, 0.4 mmol) and **7a** (0.12 g, 0.2 mmol) and by using hydrochloric acid for lyophilization (10 mM, 70 mL). Yield: 0.19 g (70%). Anal. ($C_{27}H_{26}Cl_3N_3ORuS·1.5H_2O$): C, H, N, S, Cl.

*T-4-R/S-[3-(1H-Benzimidazol-2-yl-κN$^{3'}$)-1H-quinoxalin-2-one-κN^4]-chlorido-(η^6-1-isopropyl-4-methylbenzene)-osmium(II) Chloride (**9a**).* The complex was prepared according to procedure C starting from **4a** (0.11 g, 0.4 mmol) and **7b** (0.16 g, 0.2 mmol). Diethyl ether (70 mL) was used for precipitation and hydrochloric acid (10 mM, 50 mL) for lyophilization. Yield: 0.13 g (46%). Anal. ($C_{25}H_{24}Cl_2N_4OOs·2H_2O$): C, H, N.

*T-4-R/S-[3-(Benzoxazol-2-yl-κN$^{3'}$)-1H-quinoxalin-2-one-κN^4]-chlorido-(η^6-1-isopropyl-4-methylbenzene)-osmium(II) Chloride (**9h**).* The complex was prepared according to procedure C starting from **4h** (0.16 g, 0.6 mmol) and **7b** (0.24 g, 0.3 mmol). Diethyl ether (17 mL) was used for precipitation and hydrochloric acid (10 mM, 70 mL) for lyophilization. Yield: 0.33 g (77%). Anal. ($C_{25}H_{23}Cl_2N_3O_2Os·2H_2O$): C, H, N.

*T-4-R/S-[3-(Benzothiazol-2-yl-κN$^{3'}$)-1H-quinoxalin-2-one-κN^4]-chlorido-(η^6-1-isopropyl-4-methylbenzene)-osmium(II) Chloride (**9l**).* The complex was prepared according to general procedure B starting from **4l** (0.11 g, 0.4 mmol) and **7b** (0.16 g, 0.2 mmol). Hydrochloric acid (10 mM, 100 mL) was used for lyophilization. Yield: 0.17 g (60%). Anal. ($C_{25}H_{23}Cl_2N_3OOsS·1.5H_2O$): C, H, N, S.

*T-4-R/S-(η^6-Benzene)-[3-(1H-benzimidazol-2-yl-κN$^{3'}$)-1H-quinoxalin-2-one-κN^4]-chlorido-ruthenium(II) Chloride (**10a**).* To a suspension of **4a** (0.26 g, 1.0 mmol) in absolute ethanol (7 mL) was added bis[(η^6-benzene)chlorido(μ-chlorido)ruthenium(II)] (0.25 g, 0.5 mmol). The mixture was stirred at 80 °C for 15 min and then under argon and light protection at room temperature for 90 min. Subsequently, the solid was filtered off and washed with ethanol (3 mL) and acetone (3 × 10 mL). After drying, the crude material was dissolved in water (500 mL), the turbid solution filtered, the clear filtrate immediately frozen, and lyophilized. Yield: 0.35 g (64%). Anal. ($C_{21}H_{16}Cl_2N_4ORu·2H_2O$): C, H, N, Cl.

■ ASSOCIATED CONTENT

Ⓢ Supporting Information

Synthetic procedures of precursors, spectroscopic data (^{1}H and ^{13}C NMR, mass spectra, IR and UV−vis spectra) and microanalytical data of all novel compounds, which were screened for antiproliferative activity, crystallographic data in CIF format, details of X-ray data collection and refinement, results of X-ray diffraction studies (numbering schemes and packing), and concentration-effect curves of MTT assays. This material is available free of charge via the Internet at http://pubs.acs.org.

■ AUTHOR INFORMATION

Corresponding Author

*Phone: +431427752600. Fax: +431427752680. E-mail: vladimir.arion@univie.ac.at (V.B.A.); bernhard.keppler@univie.ac.at (B.K.K.).

Notes

The authors declare no competing financial interest.

■ ACKNOWLEDGMENTS

The authors are indebted to the FFG (Austrian Research Promotion Agency, project no. 811591 FA526003) and to the Austrian Council for Research and Technology Development and COST (European Cooperation in the Field of Scientific and Technical Research) for financial support. We also thank Anatoly Dobrov for ESI mass spectra measurements, Wolfgang Kandioller for NMR measurements, and Alexander Egger for carrying out some of the MTT assays. Irene Herbacek (Institute of Cancer Research, Department of Medicine I, Medical University of Vienna) is gratefully acknowledged for flow cytometry analyses of cell cycle effects, and Prof. Verena Dirsch and Daniel Schachner (both Department of Pharmacognosy, University of Vienna) for providing FACS equipment and technical assistance for flow cytometric cell death analyses.

■ REFERENCES

(1) Jakupec, M. A.; Galanski, M.; Arion, V. B.; Hartinger, C. G.; Keppler, B. K. Antitumor metal compounds: more than theme and variations. *Dalton Trans.* **2008**, 183−194.

(2) Reedijk, J. Medicinal applications of metal complexes binding to biological macromolecules. *Macromol. Symp.* **2008**, *270*, 193−201.

(3) Fricker, S. P. Metal based drugs: from serendipity to design. *Dalton Trans.* **2007**, 4903−4917.

(4) Clarke, M. J. Ruthenium metallopharmaceuticals. *Coord. Chem. Rev.* **2003**, *236*, 209−233.

(5) Bratsos, I.; Jedner, S.; Gianferrara, T.; Alessio, E. Ruthenium Anticancer Compounds: Challenges and Expectations. *Chimia* **2007**, *61*, 692−697.

(6) Rademaker-Lakhai, J. M.; Van Den Bongard, D.; Pluim, D.; Beijnen, J. H.; Schellens, J. H. M. A Phase I and Pharmacological Study with Imidazolium-*trans*-DMSO-imidazole-tetrachlororuthenate, a Novel Ruthenium Anticancer Agent. *Clin. Cancer Res.* **2004**, *10*, 3717−3727.

(7) Lentz, F.; Drescher, A.; Lindauer, A.; Henke, M.; Hilger, R. A.; Hartinger, C. G.; Scheulen, M. E.; Dittrich, C.; Keppler, B. K.; Jaehde, U. Pharmacokinetics of a novel anticancer ruthenium complex (KP1019, FFC14A) in a phase I dose-escalation study. *Anti-Cancer Drugs* **2009**, *20*, 97−103.

(8) Gianferrara, T.; Bratsos, I.; Alessio, E. A categorization of metal anticancer compounds based on their mode of action. *Dalton Trans.* **2009**, 7588−7598.

(9) Peacock, A. F. A.; Sadler, P. J. Medicinal organometallic chemistry: designing metal arene complexes as anticancer agents. *Chem. Asian J.* **2008**, *3*, 1890−1899.

(10) Suess-Fink, G. Arene ruthenium complexes as anticancer agents. *Dalton Trans.* **2010**, *39*, 1673−1688.

(11) Liu, H. K.; Berners-Price, S. J.; Wang, F.; Parkinson, J. A.; Xu, J.; Bella, J.; Sadler, P. J. Diversity in guanine-selective DNA binding modes for an organometallic ruthenium arene complex. *Angew. Chem., Int. Ed.* **2006**, *45*, 8153−8156.

(12) Wang, F.; Habtemariam, A.; van der Geer, E. P. L; Fernandez, R.; Melchart, M.; Deeth, R. J.; Aird, R.; Guichard, S.; Fabbiani, F. P. A; Lozano-Casal, P.; Oswald, I. D. H.; Jodrell, D. I.; Parsons, S.; Sadler, P. J. Controlling ligand substitution reactions of organometallic complexes: tuning cancer cell cytotoxicity. *Proc. Natl. Acad. Sci. U.S.A.* **2005**, *102*, 18269−18274.

(13) Habtemariam, A.; Melchart, M.; Fernandez, R.; Parsons, S.; Oswald, I. D. H.; Parkin, A.; Fabbiani, F. P. A; Davidson, J. E.; Dawson, A.; Aird, R. E.; Jodrell, D. I.; Sadler, P. J. Structure−Activity Relationships for Cytotoxic Ruthenium(II) Arene Complexes Containing *N,N*-, *N,O*-, and *O,O*-Chelating Ligands. *J. Med. Chem.* **2006**, *49*, 6858−6868.
(14) Dyson, P. J. Systematic design of a targeted organometallic antitumor drug in preclinical development. *Chimia* **2007**, *61*, 698−703.
(15) Scolaro, C.; Chaplin, A. B.; Hartinger, C. G.; Bergamo, A.; Cocchietto, M.; Keppler, B. K.; Sava, G.; Dyson, P. J. Tuning the hydrophobicity of ruthenium(II)−arene (RAPTA) drugs to modify uptake, biomolecular interactions and efficacy. *Dalton Trans.* **2007**, 5065−5072.
(16) Ang, W. H.; Daldini, E.; Scolaro, C.; Scopelliti, R.; Juillerat-Jeannerat, L.; Dyson, P. J. Development of Organometallic Ruthenium−Arene Anticancer Drugs That Resist Hydrolysis. *Inorg. Chem.* **2006**, *45*, 9006−9013.
(17) Pawson, T.; Kofler, M. Kinome signaling through regulated protein−protein interactions in normal and cancer cells. *Curr. Opin. Cell Biol.* **2009**, *21*, 147−153.
(18) Grant, S. K. Therapeutic Protein Kinase Inhibitors. *Cell. Mol. Life Sci.* **2009**, *66*, 1163−1177.
(19) Noble, M. E.; Endicott, J. A.; Johnson, L. N. Protein kinase inhibitors: insights into drug design from structure. *Science* **2004**, *303*, 1800−1805.
(20) Bregman, H.; Williams, D. S.; Atilla, G. E.; Carroll, P. J.; Meggers, E. An Organometallic Inhibitor for Glycogen Synthase Kinase 3. *J. Am. Chem. Soc.* **2004**, *126*, 13594−13595.
(21) Maksimoska, J.; Feng, L.; Harms, K.; Yi, C.; Kissil, J.; Marmorstein, R.; Meggers, E. Targeting Large Kinase Active Site with Rigid, Bulky Octahedral Ruthenium Complexes. *J. Am. Chem. Soc.* **2008**, *130*, 15764−15765.
(22) Atilla-Gokcumen, G. E.; Pagano, N.; Streu, C.; Maksimoska, J.; Filippakopoulos, P.; Knapp, S.; Meggers, E. Extremely Tight Binding of a Ruthenium Complex to Glycogen Synthase Kinase 3. *ChemBioChem* **2008**, *9*, 2933−2936.
(23) Meggers, E. Targeting proteins with metal complexes. *Chem. Commun.* **2009**, 1001−1010.
(24) Bikker, J. A.; Brooijmans, N.; Wissner, A.; Mansour, T. S. Kinase Domain Mutations in Cancer: Implications for Small Molecule Drug Design Strategies. *J. Med. Chem.* **2009**, *52*, 1493−1509.
(25) Hoessel, R.; Leclerc, S.; Endicott, J. A.; Noble, M. E. M.; Lawrie, A.; Tunnah, P.; Leost, M.; Damiens, E.; Marie, D.; Marko, D.; Niederberger, E.; Tang, W.; Eisenbrand, G.; Meijer, L. Indirubin, the active constituent of a Chinese antileukaemia medicine, inhibits cyclin-dependent kinases. *Nature Cell Biol.* **1999**, *1*, 60−67.
(26) Eisenbrand, G.; Hippe, F.; Jakobs, S.; Muehlbeyer, S. Molecular mechanisms of indirubin and its derivatives: novel anticancer molecules with their origin in traditional Chinese phytomedicine. *J. Cancer Res. Clin. Oncol.* **2004**, *130*, 627−635.
(27) Nam, S.; Buettner, R.; Turkson, J.; Kim, D.; Cheng, J. Q.; Muehlbeyer, S.; Hippe, F.; Vatter, S.; Merz, K.; Eisenbrand, G.; Jove, R. Indirubin derivatives inhibit Stat3 signaling and induce apoptosis in human cancer cells. *Proc. Natl. Acad. Sci. U.S.A.* **2005**, *102*, 5998−6003.
(28) Lee, M. J.; Kim, M. Y.; Mo, J. S.; Ann, E. J.; Seo, M.-S.; Hong, J.-A.; Kim, Y.-C.; Park, H. S. Indirubin-3′-monoxime, a derivative of a Chinese anti-leukemia medicine, inhibits Notch1 signaling. *Cancer Lett.* **2008**, *265*, 215−225.
(29) Beauchard, A.; Ferandin, Y.; Frere, S.; Lozach, O.; Blairvacq, M.; Meijer, L.; Thiery, V.; Besson, T. Synthesis of novel 5-substituted indirubins as protein kinases inhibitors. *Bioorg. Med. Chem.* **2006**, *14*, 6434−6443.
(30) Jautelat, R.; Brumby, T.; Schaefer, M.; Briem, H.; Eisenbrand, G.; Schwahn, S.; Krueger, M.; Luecking, U.; Prien, O.; Siemeister, G. From the insoluble dye indirubin towards highly active, soluble CDK2-inhibitors. *ChemBioChem* **2005**, *6*, 531−540.
(31) Knockaert, M.; Blondel, M.; Bach, S.; Leost, M.; Elbi, C.; Hager, G. L.; Nagy, S. R.; Han, D.; Denison, M.; Ffrench, M.; Ryan, X. P.; Magiatis, P.; Polychronopoulos, P.; Greengard, P.; Skaltsounis, L.; Meijer, L. Independent actions on cyclin-dependent kinases and aryl hydrocarbon receptor mediate the antiproliferative effects of indirubins. *Oncogene* **2004**, *23*, 4400−4412.
(32) Siemeister, G.; Thierauch, K. H.; Prien, O.; Jautelat, R.; Eisenbrand, G. Therapeutic use of selective indirubin derivatives as VEGF receptor inhibitors. Int. PatentWO 02/092079 A1, November 21, 2002.
(33) Davies, T. G.; Tunnah, P.; Meijer, L.; Marko, D.; Eisenbrand, G.; Endicott, J. A.; Noble, M. E. M. Inhibitor Binding to Active and Inactive CDK2 The Crystal Structure of CDK2-Cyclin A/ Indirubin-5-Sulphonate. *Structure* **2001**, *9*, 389−397.
(34) Renhowe, P.; Pecchi, S.; Machajewski, T.; Shafer, C.; Taylor, C.; McCrea, B.; McBride, C.; Jazan, E.; Wernette-Hammond, M. E.; Harris, A. Quinolinone Derivatives as Tyrosine Kinase Inhibitors. Int. Patent WO 02/22598 A1, March 21, 2002.
(35) Frazier, K.; Jazan, E.; McBride, C. M.; Pecchi, S.; Renhowe, P. A.; Shafer, C. M.; Taylor, C.; Bussiere, D.; Min, He M.; Jansen, J. M.; Lapointe, G.; Ma, S.; Vora, J.; Wiesmann, M. Design and structure−activity relationship of heterocyclic analogs of 4-amino-3-benzimidazol-2-ylhydroquinolin-2-ones as inhibitors of receptor tyrosine kinases. *Bioorg. Med. Chem. Lett.* **2006**, *16*, 2247−2251.
(36) Renhowe, P. A.; Pecchi, S.; Shafer, C. M.; Machajewski, T. D.; Jazan, E. M.; Taylor, C.; Antonios-McCrea, W.; McBride, C. M.; Frazier, K.; Wiesmann, M.; Lapointe, G. R.; Feucht, P. H.; Warne, R. L.; Heise, C. C.; Menezes, D.; Aardalen, K.; Ye, H.; He, M.; Le, V.; Vora, J.; Jansen, J. M.; Wernette-Hammond, M. E.; Harris, A. L. Design, Structure−Activity Relationships and in Vivo Characterization of 4-Amino-3-benzimidazol-2-ylhydroquinolin-2-ones: A Novel Class of Receptor Tyrosine Kinase Inhibitors. *J. Med. Chem.* **2009**, *52*, 278−292.
(37) Ladouceur, G. H.; Bear, B.; Bi, C.; Brittelli, D. R.; Burke, M. J.; Chen, G.; Cook, J.; Dumas, J.; Sibley, R.; Turner, M. R. Indolyl pyrazinone derivatives useful for treating hyper-proliferative disorders and diseases associated with angiogenesis. Int. Patent WO 2004/043950 A1, May 27, 2004.
(38) Aoki, K.; Koseki, J.; Takeda, S.; Aburada, M.; Miyamoto, K. Convenient synthetic method for 3-(3-substituted indol-2-yl)-quinoxalin-2-ones as VEGF inhibitor. *Chem. Pharm. Bull.* **2007**, *55*, 922−925.
(39) Westphal, G.; Scheybal, A.; Lipke, B.; Weber, F. G. Reactions with pyridinium pyruvates. *Pharmazie* **1976**, *31*, 770−773.
(40) Westphal, G.; Scheybal, A.; Lipke, B.; Weber, F. G. Preparation of several 3-hetaryl-2-quinoxalinones. *Pharmazie* **1977**, *32*, 563−565.
(41) Klicnar, J.; Hajek, M.; Dobas, I. Quinoxaline series. III. Synthesis, reactions, and infrared spectra of some 3-hydroxy-2-carboxymethylquinoxaline derivatives. *Collect. Czech. Chem. Commun.* **1965**, *30*, 3092−3101.
(42) Kandioller, W.; Hartinger, C. G.; Nazarov, A. A.; Kasser, J.; John, R.; Jakupec, M. A.; Arion, V. B.; Dyson, P. J.; Keppler, B. K. Tuning the anticancer activity of maltol-derived ruthenium complexes by derivatization of the 3-hydroxy-4-pyrone moiety. *J. Organomet. Chem.* **2009**, *694*, 922−929.
(43) Kandioller, W.; Hartinger, C. G.; Nazarov, A. A.; Kuznetsov, M. L.; John, R. O.; Bartel, C.; Jakupec, M. A.; Arion, V. B.; Keppler, B. K. From Pyrone to Thiopyrone Ligands—Rendering Maltol-Derived Ruthenium(II)−Arene Complexes That Are Anticancer Active in Vitro. *Organometallics* **2009**, *28*, 4249−4251.
(44) Canivet, J.; Karmazin-Brelot, L.; Suess-Fink, G. Cationic arene ruthenium complexes containing chelating 1,10-phenanthroline ligands. *J. Organomet. Chem.* **2005**, *690*, 3202−3211.
(45) Wang, F.; Chen, H.; Parsons, S.; Oswald, I. D. H.; Davidson, J. E.; Sadler, P. J. Kinetics of aquation and anation of ruthenium(II) arene anticancer complexes, acidity and X-ray structures of aqua adducts. *Chem.—Eur. J.* **2003**, *9*, 5810−5820.
(46) Peacock, A. F. A.; Habtemariam, A.; Fernandez, R.; Walland, V.; Fabbiani, F. P. A; Parsons, S.; Aird, R. E.; Jodrell, D. I.; Sadler, P. J. Tuning the Reactivity of Osmium(II) and Ruthenium(II) Arene

Complexes under Physiological Conditions. *J. Am. Chem. Soc.* **2006**, *128*, 1739−1748.
(47) Santra, S.; Dogra, S. K. Solvatochromism and prototropic reactions of 2-quinoxalinone. *Chem. Phys.* **1996**, *207*, 103−113.
(48) Dadci, L.; Elias, H.; Frey, U.; Hoernig, A.; Koelle, U.; Merbach, A. E.; Paulus, H.; Schneider, J. S. π-Arene Aqua Complexes of Cobalt, Rhodium, Iridium, and Ruthenium: Preparation, Structure, and Kinetics of Water Exchange and Water Substitution. *Inorg. Chem.* **1995**, *34*, 306−315.
(49) Peacock, A. F. A.; Habtemariam, A.; Moggach, S. A.; Prescimone, A.; Parsons, S.; Sadler, P. J. Chloro half-sandwich osmium(II) complexes: influence of chelated *N*,*N*-ligands on hydrolysis, guanine binding, and cytotoxicity. *Inorg. Chem.* **2007**, *46*, 4049−4059.
(50) Damiens, E.; Baratte, B.; Marie, D.; Eisenbrand, G.; Meijer, L. Anti-mitotic properties of indirubin-3′-monoxime, a CDK/GSK-3 inhibitor: induction of endoreplication following prophase arrest. *Oncogene* **2001**, *20*, 3786−3797.
(51) Ginzinger, W.; Egger, A.; Mühlgassner, G.; Arion, V. B.; Jakupec, M. A.; Galanski, M.; Berger, W.; Keppler, B. K. Water soluble indirubin derivatives with a quaternary ammonium moiety. Manuscript in preparation.
(52) Bennett, M. A.; Smith, A. K. Arene ruthenium(II) complexes formed by dehydrogenation by cyclohexadienes with ruthenium(III) trichloride. *J. Chem. Soc., Dalton Trans.* **1974**, 233−241.
(53) Hodson, E.; Simpson, S. J. Synthesis and characterization of $[(\eta^6\text{-cymene})Ru(L)X_2]$ compounds: single crystal X-ray structure of $[(\eta^6\text{-cymene})Ru(P\{OPh\}_3)Cl_2]$ at 203 K. *Polyhedron* **2004**, *23*, 2695−2707.
(54) Kiel, W. A.; Ball, R. G.; Graham, W. A. G. Carbonyl-η-hexamethylbenzene complexes of osmium. Carbon−hydrogen activation by $(\eta\text{-}C_6Me_6)Os(CO)(H)_2$. *J. Organomet. Chem.* **1990**, *383*, 481−496.
(55) Brauer, G.; Fehlhammer, W. P.; Glemser, O.; Grube, H. J.; Gustav, K.; Herrmann, W. A.; Herzog, S.; Lux, H.; Müller, H.; Ofele, K.; Schill, E.; Scholdert, R.; Schwärzt, H.; Schwarzmann, E.; Schwochau, K.; Simon, A.; Strähle, J. In *Handbuch der Präparativen Anorganischen Chemie*, 3rd ed.; Brauer, G., Ed.; Ferdinand Enke Verlag: Stuttgart, 1981; Vol. 3, p 1743.
(56) Pressprich, M. R.; Chambers, J. *SAINT-Plus Integration Engine, Program for Crystal Structure Integration*; Bruker AXS Inc.: Madison, WI, 2004.
(57) Sheldrick, G. M. *SHELXS-97, Program for Crystal Structure Solution*; University Göttingen: Göttingen, 1997.
(58) Farrugia, L. J. WinGX suite for small-molecule single-crystal crystallography. *J. Appl. Crystallogr.* **1999**, *32*, 837−838.
(59) Sheldrick, G. M. *SHELXL-97, Program for Crystal Structure Refinement*; University Göttingen: Göttingen, 1997.
(60) Spek, A. L. Single-crystal structure validation with the program *PLATON*. *J. Appl. Crystallogr.* **2003**, *36*, 7−13.
(61) Bruker, A. *XP-Interactive Molecular Graphics, version 5.1*; Bruker AXS Inc.: Madison, WI, 1998.
(62) *International Tables for X-ray Crystallography*; Kluwer Academic Press: Dodrecht, The Netherlands, 1992; Vol. *C*, Tables 4.2.6.8 and 6.1.1.4.
(63) Mosmann, T. J. Rapid colorimetric assay for cellular growth and survival: application to proliferation and cytotoxicity assays. *J. Immunol. Methods* **1983**, *65*, 55−63.
(64) Aubry, J.-P.; Blaecke, A.; Lecoanet-Henchoz, S.; Jeannin, P.; Herbault, N.; Caron, G.; Moine, V.; Bonnefoy, J.-Y. *Cytometry* **1999**, *37*, 197−204.
(65) Eller, G. A.; Datterl, B.; Holzer, W. Pyrazolo[4′,3′:5,6]pyrano-[2,3-*b*]quinoxalin-4(1*H*)-one: synthesis and characterization of a novel tetracyclic ring system. *J. Heterocycl. Chem.* **2007**, *44*, 1139−1143.